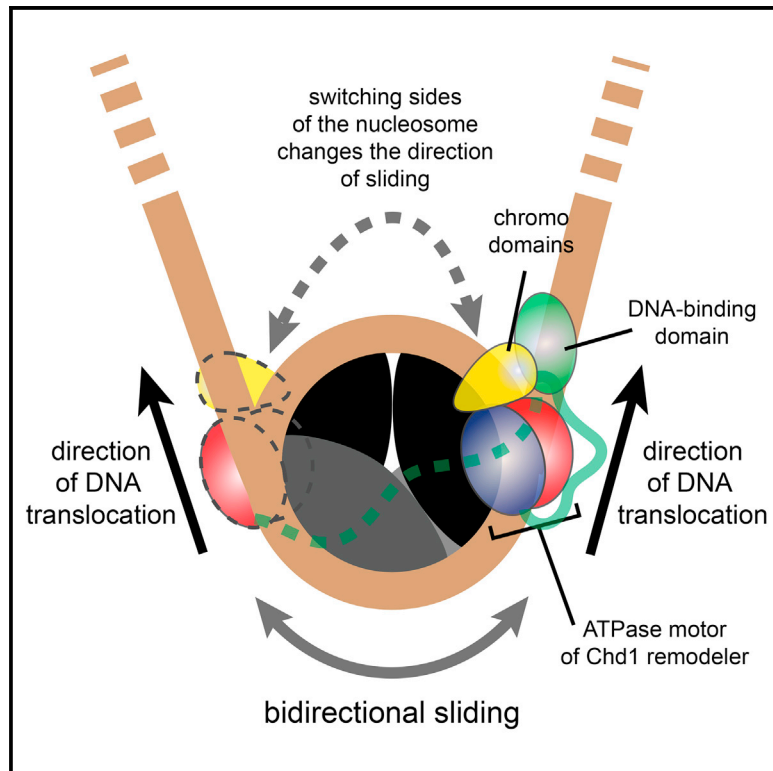


The Chd1 Chromatin Remodeler Shifts Nucleosomal DNA Bidirectionally as a Monomer

Graphical Abstract



Authors

Yupeng Qiu, Robert F. Levendosky, Srinivas Chakravarthy, Ashok Patel, Gregory D. Bowman, Sua Myong

Correspondence

gdbowman@jhu.edu (G.D.B.),
smyong@jhu.edu (S.M.)

In Brief

Chd1 is an ATP-driven chromatin remodeler that evenly repositions nucleosomes along DNA. Qiu et al. demonstrate that a single Chd1 molecule can dynamically shift nucleosomes back and forth. Such bidirectional activity is tightly controlled by two regulatory domains that guide nucleosome sliding and substrate selection.

Highlights

- Monomeric Chd1 exhibits dynamic shifting of nucleosomal DNA back and forth
- Bidirectional sliding by Chd1 entails unstable remodeling intermediates
- Limiting the range of the Chd1 DBD interferes with nucleosome sliding
- N-terminal chromodomains of Chd1 guard against sliding hexasomes



The Chd1 Chromatin Remodeler Shifts Nucleosomal DNA Bidirectionally as a Monomer

Yupeng Qiu,^{1,2} Robert F. Levendosky,¹ Srinivas Chakravarthy,³ Ashok Patel,⁴ Gregory D. Bowman,^{1,*} and Sua Myong^{1,2,5,6,*}

¹Department of Biophysics, Johns Hopkins University, Baltimore, MD 21218, USA

²Department of Bioengineering, University of Illinois, Urbana, IL 61801, USA

³Biophysics Collaborative Access Team, Argonne National Laboratory, Argonne, IL 60439, USA

⁴Kusuma School of Biological Sciences, Indian Institute of Technology Delhi, Hauz Khas, New Delhi 110016, India

⁵Physics Frontier Center (Center for Physics of Living Cells), University of Illinois, Urbana, IL 61801, USA

⁶Lead Contact

*Correspondence: gdbowman@jhu.edu (G.D.B.), smyong@jhu.edu (S.M.)

<http://dx.doi.org/10.1016/j.molcel.2017.08.018>

SUMMARY

Chromatin remodelers catalyze dynamic packaging of the genome by carrying out nucleosome assembly/disassembly, histone exchange, and nucleosome repositioning. Remodeling results in evenly spaced nucleosomes, which requires probing both sides of the nucleosome, yet the way remodelers organize sliding activity to achieve this task is not understood. Here, we show that the monomeric Chd1 remodeler shifts DNA back and forth by dynamically alternating between different segments of the nucleosome. During sliding, Chd1 generates unstable remodeling intermediates that spontaneously relax to a pre-remodeled position. We demonstrate that nucleosome sliding is tightly controlled by two regulatory domains: the DNA-binding domain, which interferes with sliding when its range is limited by a truncated linking segment, and the chromodomains, which play a key role in substrate discrimination. We propose that active interplay of the ATPase motor with the regulatory domains may promote dynamic nucleosome structures uniquely suited for histone exchange and chromatin reorganization during transcription.

INTRODUCTION

Chromatin remodelers are specialized ATP-dependent DNA translocases that can reposition, evict, and replace histones within the nucleosome (Narlikar et al., 2013). The need for such activities arises from the compact organization of chromosomal DNA into nucleosomes that requires accessibility for essential genomic processes, such as replication, transcription, and DNA repair. Subsequent to such disruptive events, chromatin needs to be properly repackaged to maintain genomic integrity. Accomplishing these tasks requires multiple families of remodelers that are specialized for achieving particular remodeling

outcomes. Each remodeler family can be identified by unique regulatory domains that determine substrate specificities and control action of a conserved helicase-like ATPase motor. The interplay of regulatory domains with the ATPase motor occurs in the context of temporally regulated epigenetic modifications critical for cellular differentiation, development, and human diseases. As exemplified by the Chd1 chromatin remodeler, disruption of individual remodelers can have profound consequences, such as loss of stem cell pluripotency or stimulation of cancer cell proliferation (Burkhardt et al., 2013; Gaspar-Maia et al., 2009; Zhao et al., 2017).

Action of the Chd1 remodeler is tightly coupled to transcription, as evidenced by direct interaction of Chd1 with several elongation factors (Kelley et al., 1999; Krogan et al., 2002; Simic et al., 2003), subunits of mediator and the spliceosome (Lin et al., 2011; Sims et al., 2007), and, in metazoans, the histone H3K4 methylation mark (Flanagan et al., 2005). Chd1 catalyzes both nucleosome assembly and array spacing (Fei et al., 2015; Gkikopoulos et al., 2011; Lusser et al., 2005), which are important in re-establishing the chromatin barrier after passage of RNA polymerase II (Smolle et al., 2012). Additionally, Chd1 has also been shown to facilitate or be required for exchange of histone H3 variants (Konev et al., 2007), a poorly understood process that requires significant structural reorganization of histone-DNA interactions.

Chd1 possesses two prominent regulatory domains: a sequence nonspecific DNA-binding domain (DBD) located C-terminal to the ATPase motor and a pair of chromodomains immediately N-terminal to the ATPase motor. A crystal structure of the chromo-ATPase portion of Chd1 showed that the chromodomains can directly block a DNA-binding surface of the ATPase motor via an acidic helix (Hauk et al., 2010). This interaction appears autoinhibitory, as disruption of this interface increased ATPase stimulation by naked DNA and recovered sliding of nucleosomes lacking the H4 tail (Hauk et al., 2010). Whereas these activities are consistent with the chromodomains serving as a selectivity filter, it has been unclear what natural nucleosome substrates may be blocked by chromodomain inhibition.

The DBD of Chd1 was initially found to have an important role in tethering the remodeler to nucleosome substrates. Deletion of the DBD severely impaired nucleosome sliding activity, yet substituting foreign binding domains restored robust

sliding, indicating that the DBD is not mechanically required for nucleosome repositioning (McKnight et al., 2011; Nodelman and Bowman, 2013; Patel et al., 2013). More recently, the finding that the DBD communicates with the ATPase motor when bound to DNA flanking the nucleosome has suggested that the DBD also plays a regulatory role (Nodelman et al., 2017). Like SWItch/Sucrose Non-Fermentable (SWI/SNF) and imitation switch (ISWI) remodelers, the ATPase motor of Chd1 translocates on DNA at superhelix location 2 (SHL2), an internal site ~ 20 bp from the nucleosome dyad (McKnight et al., 2011; Saha et al., 2005; Schwanbeck et al., 2004; Zofall et al., 2006). DNA translocation by these remodeler ATPases is believed to be unidirectional, and therefore, relative to the SHL2 site where the ATPase motor is engaged, DNA flanking one side of the nucleosome shifts onto the core (entry side) while DNA on the other turn or gyre of DNA shifts further away from the nucleosome core (exit side). The ATPase motor and DBD of Chd1 can therefore be in two distinct organizations on the nucleosome: they can be either on opposite DNA gyres and spatially close together on the same “edge” of the nucleosome or on the same DNA gyre and separated from each other across the face of the nucleosome (Nodelman et al., 2017). When on the same gyre and across the face of the nucleosome, the DBD can assist the ATPase motor via tethering but would be too far to directly contact the ATPase motor. As shown with Chd1 fusion remodelers (McKnight et al., 2011; Patel et al., 2013), this separated organization is stimulating. In contrast, when the DBD and ATPase are on opposite DNA gyres and therefore physically close, these domains can communicate with each other. As suggested by faster nucleosome sliding away from Lac repressor and dampening of ATPase activity (Nodelman et al., 2016, 2017), this cross-gyre communication appears to interfere with nucleosome sliding. The dynamics by which Chd1 switches between active and inhibited states has not previously been examined.

In this study, we took advantage of a single-molecule fluorescence approach to dissect the nucleosome sliding activity of Chd1. Our results reveal that Chd1 repositions nucleosomes in a stepwise manner, dependent on ATP hydrolysis. Surprisingly, we discovered that Chd1 shifts nucleosomal DNA back and forth as a monomer. ATP-dependent translocation of DNA was consistently followed by ATP-independent reversals, resulting in the DNA snapping back to a previous position. We believe this behavior reveals unstable remodeling intermediates, which provide potential checkpoints for regulatory elements. By mutational analysis, we investigated roles of both the chromodomains and DBD. We discovered that the chromodomains are responsible for blocking hexasome sliding and therefore provide a critical safeguard against sliding incomplete nucleosomes. We also found that deletion of a linker segment between the ATPase motor and DBD, previously shown to have virtually no sliding activity (Nodelman and Bowman, 2013), yields dynamic but unstable movement of exit-side DNA, suggesting active inhibition due to the DBD. Taken together, our results reveal dynamic action and regulation of Chd1 that are likely central for assembling and evenly spacing nucleosomes throughout the genome.

RESULTS

Chd1 Repositions the Nucleosome in a Stepwise Manner

Following the single-molecule design from a previous study (Deindl et al., 2013), we generated fluorescence resonance energy transfer (FRET)-labeled nucleosomes to study remodeling by Chd1. Using the Widom 601 positioning sequence (Lowary and Widom, 1998), we prepared end-positioned nucleosomes (called 3N80), with the short 3-bp end labeled with Cy3, which is close enough to FRET with Cy5 on the H2A C terminus (T120C; Figure 1A; Li and Widom, 2004). The 80-bp side of the DNA was biotinylated for immobilization to a NeutrAvidin-coated polyethylene glycol (PEG) surface (Ngo et al., 2015; Roy et al., 2008), and movement of the short end away from the histone core is reported by a decrease in FRET (Deindl et al., 2013). For single-molecule detection, we added 100 pM of FRET-labeled nucleosome to the surface, which yielded approximately 400 spatially separated FRET spots in one field of view ($25 \times 75 \mu\text{m}^2$).

Chd1 (20 nM) and ATP (1 mM) were added in succession to FRET-labeled nucleosomes immobilized on the PEGylated surface. Fifteen to twenty images were taken, and the FRET values collected from 6,000–8,000 molecules were built into a FRET histogram. The major peak appears at high FRET of 0.9, as expected from the proximity between the Cy3 and Cy5 dyes (Figure 1B, top). A minor mid-FRET peak at 0.6 is likely due to the Cy5-labeled H2A at a distal position, as seen in previous studies (Deindl et al., 2013; Levendosky et al., 2016). FRET peaks did not change upon addition of Chd1 protein alone without ATP (Figure 1B, middle). When ATP was added, all molecules shifted to low FRET (0.1; Figure 1B, bottom), indicating that nucleosome repositioning by Chd1 was ATP dependent.

Consistent with the FRET histograms, the representative single-molecule FRET traces show a steady high-FRET signal for nucleosome alone and after addition of Chd1 without nucleotide (Figure 1C, top and middle). Immediately after addition of ATP (blue arrow), the high FRET transitioned to low FRET, indicating that Chd1 repositioned nucleosomes. A closer examination of single-molecule traces revealed individual FRET steps, denoted by red arrows (Figure 1C, bottom). To reduce the stepping rate, repositioning activity was tested at varying ATP concentrations. The result was analyzed by collecting FRET values corresponding to the repositioning activity (0.9 to 0.1) from over 100 single-molecule traces at different ATP concentrations and plotting the average FRET signal over time (Figure 1D, left). As expected, the rate of FRET decrease is the highest ($\sim 0.75/\text{s}$) at 1 mM ATP and substantially lower at 5–10 μM ($\sim 0.25/\text{s}$). Based on the calculated rate, we plotted the ATP-dependent repositioning rate and fit to the Michaelis-Menten equation to determine V_{max} and K_{M} (Figure 1D, right). To improve the resolution of the stepwise FRET change, we performed the same measurement with low ATP concentrations (1–5 μM). Here, we observed three distinct steps of FRET values as indicated by red arrows (Figure 1E). We collected individual FRET values from over 100 traces and plotted as a transition density plot in which the x and y axes represent FRET values before and after a transition, respectively. This analysis shows that Chd1 takes discrete steps represented by FRET transition from 0.9 to 0.65, 0.65 to 0.4, and 0.4 to 0.1 in succession (Figure 1F). As this behavior is analogous

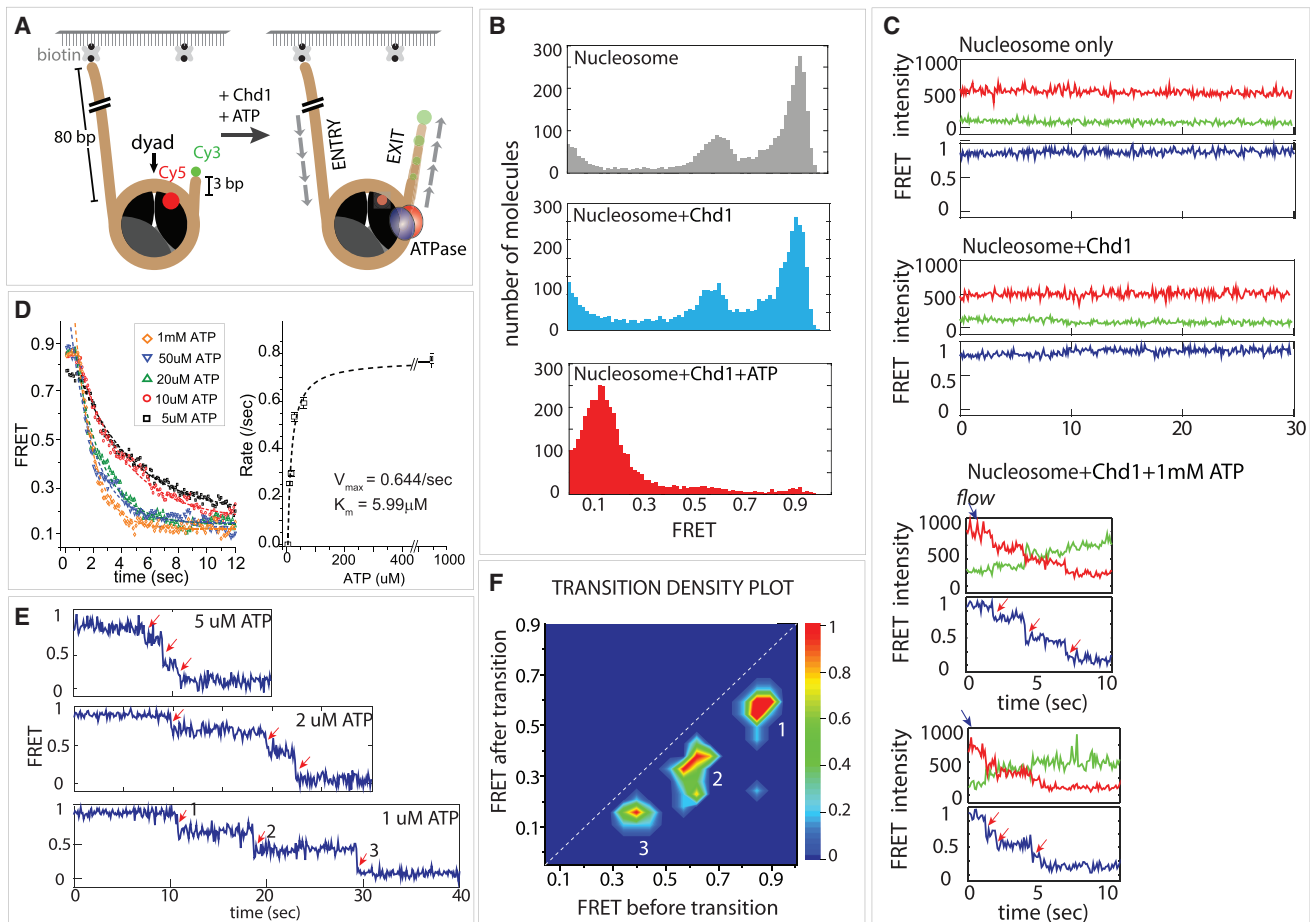


Figure 1. Chd1 Repositions the Nucleosome in a Stepwise Manner

(A) Nucleosome-FRET construct was labeled with Cy3 on exit side DNA and Cy5 on histone H2A (T120C). Only the proximal Cy5 dye is shown.

(B) Histograms of FRET values before and after addition of Chd1. FRET histograms of nucleosomes alone displayed a bimodal distribution, correlating with nucleosomes having labeled H2A in a proximal (high FRET) or distal (mid-FRET) position (gray, top). Addition of Chd1 without nucleotide (light blue, middle) did not show significant differences from nucleosome alone. After addition of ATP (red, bottom), FRET histograms were dominated by a single, low-FRET peak.

(C) Representative single-molecule FRET traces for each condition in (B).

(D) Averaged FRET traces at varying ATP concentrations and the corresponding Michaelis-Menten fit.

(E) Single-molecule traces at low ATP, which display stepwise decreases in FRET.

(F) Transition density plot showing three steps of discrete FRET transitions.

to the stepping previously observed for ISWI remodelers (Deindl et al., 2013), these data suggest that Chd1 shifts DNA past the nucleosome core in bursts of multiple base pairs.

Monomeric Chd1 Is Sufficient for Shifting Nucleosomal DNA Back and Forth

After reaching a low FRET state (0.1), we noticed a prominent pattern of FRET fluctuation in a significant fraction of single-molecule traces, suggesting movement of DNA in the opposite direction following the initial repositioning (Figure 2A). We interpret the regain in FRET as movement of the short DNA end back toward the nucleosome core. Given that nucleosomes possess 2-fold symmetry, one possible explanation for the back-and-forth motion could be alternating action of Chd1 on either side of the nucleosome. In these experiments, we flushed away excess Chd1 protein upon addition of ATP, yet it was

possible that, after initial exposure to Chd1, nucleosomes retained a Chd1 molecule on each side. An alternative possibility was that a single Chd1 molecule could also achieve bidirectional sliding, which would require that the ATPase motor hop to different nucleosome locations without dissociation of the remodeler. To determine whether a single Chd1 protein could stimulate bidirectional motion of nucleosomal DNA, we performed sliding reactions with freely diffusing nucleosomes and immobilized Chd1. Following a successful strategy from our previous studies (Hwang et al., 2014a, 2014b; Qiu et al., 2013; Tippiana et al., 2014), we tethered Chd1 to the surface using a FLAG:anti-FLAG interaction, which provided the advantage of observing activities of single Chd1 proteins. With this arrangement, the nucleosomes had the same FRET labeling scheme but were non-biotinylated, and therefore, no fluorescence signals were detected until nucleosomes bound to

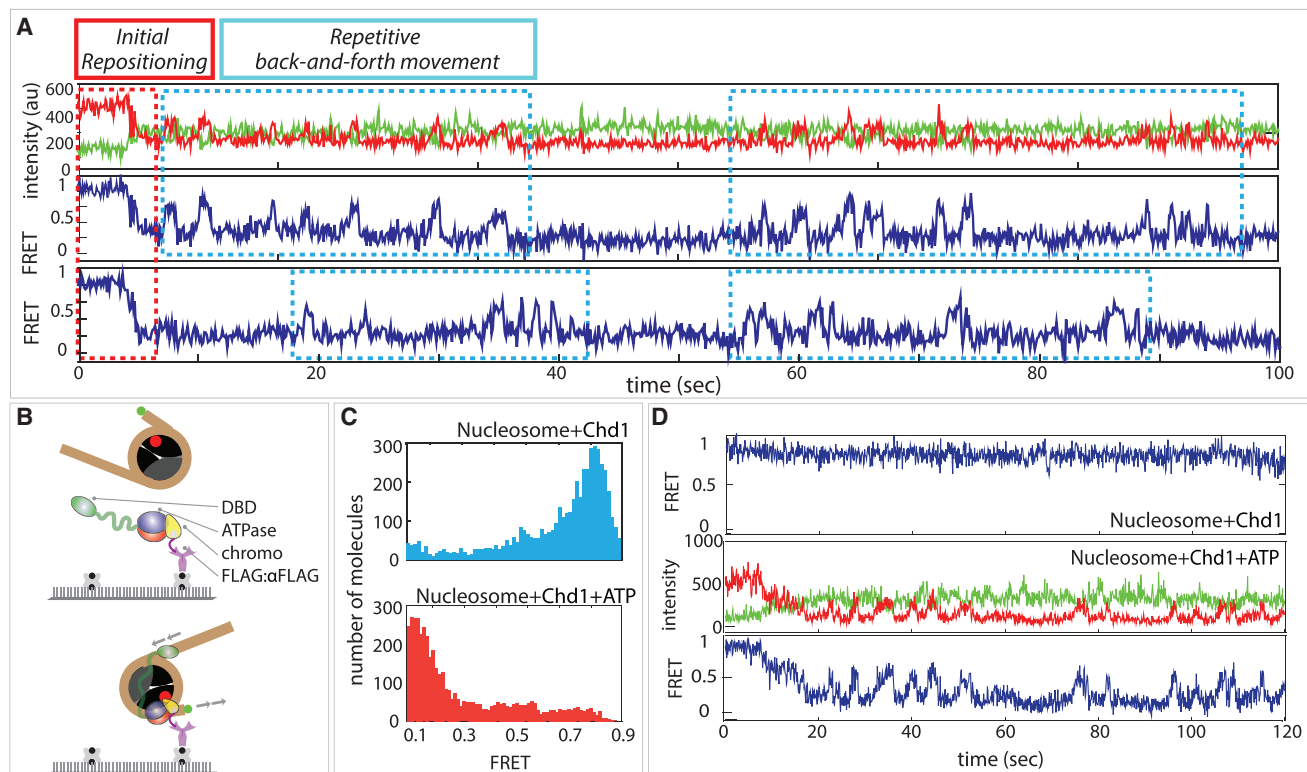


Figure 2. Chd1 Monomer Is Sufficient for Repositioning Single Nucleosomes Back and Forth

(A) Single-molecule traces of biotin-tethered nucleosomes, displaying initial repositioning (decrease in FRET) followed by repetitive increases in FRET, signifying sliding in the opposite direction.
 (B) Schematic of surface-immobilized Chd1 and FRET-labeled nucleosome applied to single-molecule platform.
 (C) FRET histograms of non-biotinylated nucleosomes with surface-immobilized Chd1 before and after ATP addition.
 (D) Single-molecule traces of FRET-labeled nucleosomes bound to surface-immobilized Chd1 before (top) and after (middle, bottom) ATP addition.

surface-immobilized Chd1 (Figure 2B). The FRET histogram taken after adding FRET-labeled nucleosome showed a FRET peak at around 0.8–0.9 (Figure 2C, top), similar to the original experiment shown in Figure 1B. These FRET signals obtained in the absence of ATP confirm that nucleosome binding to Chd1 does not rely on ATP. Upon addition of ATP, FRET decreased to low levels as before (Figure 2C, bottom). The nearly complete shift in FRET histogram signified that the majority of nucleosomes that engaged with the surface-bound Chd1 underwent active repositioning. As expected, the FRET signals remained high when nucleosomes bound Chd1 in the absence of ATP (Figure 2D, top). Remarkably, the single-molecule FRET traces taken in ATP showed the same pattern of initial FRET decrease followed by periodic regain and loss of FRET (Figure 2D, bottom). This bidirectional movement of DNA relative to the histone core indicates that, even as a monomer, Chd1 can reverse the direction of DNA translocation without dissociation.

Bidirectional Sliding Reveals Unstable Remodeling Intermediates

After reaching a low FRET state (0.1), continuous FRET fluctuations were observed where the highest level achieved was typically ~ 0.7 , which was lower than the initial FRET (~ 0.9). Such FRET fluctuations, which we interpret as a back-and-forth

motion of DNA relative to the histone core, typically occurred many times in succession (Figure 2A). Analysis of 2,000 traces over a 15-min period showed that approximately 30% of molecules exhibited a fluctuating FRET pattern, indicating that the activity was continuous (Figure 3A).

The higher percentage of FRET fluctuation in the early phases of the remodeling reaction (0–3 min) may result from more nucleosomes being closer to the starting position, where FRET is most sensitive. As the nucleosomes are distributed along the DNA in subsequent times (3–12 min), most would be beyond the FRET-detectable range.

Interestingly, we observed an asymmetric shape of the FRET fluctuations, where FRET increased gradually and decreased rapidly. This asymmetry was even more pronounced at low ATP concentrations ($\leq 5 \mu\text{M}$), which only slowed down the increase in FRET without affecting the sudden FRET drop (Figure 3B). This behavior suggests that the gradual FRET increase was ATP dependent whereas the abrupt FRET decrease was ATP independent. We calculated the frequency of this repetitive sliding by taking the inverse of time intervals corresponding to FRET increase, denoted by a double arrow (Figure 3B, top trace). The rates collected from over 1,000 molecules under varying ATP concentrations were plotted against ATP concentration and fitted to the Michaelis-Menten equation, which yielded a K_M of

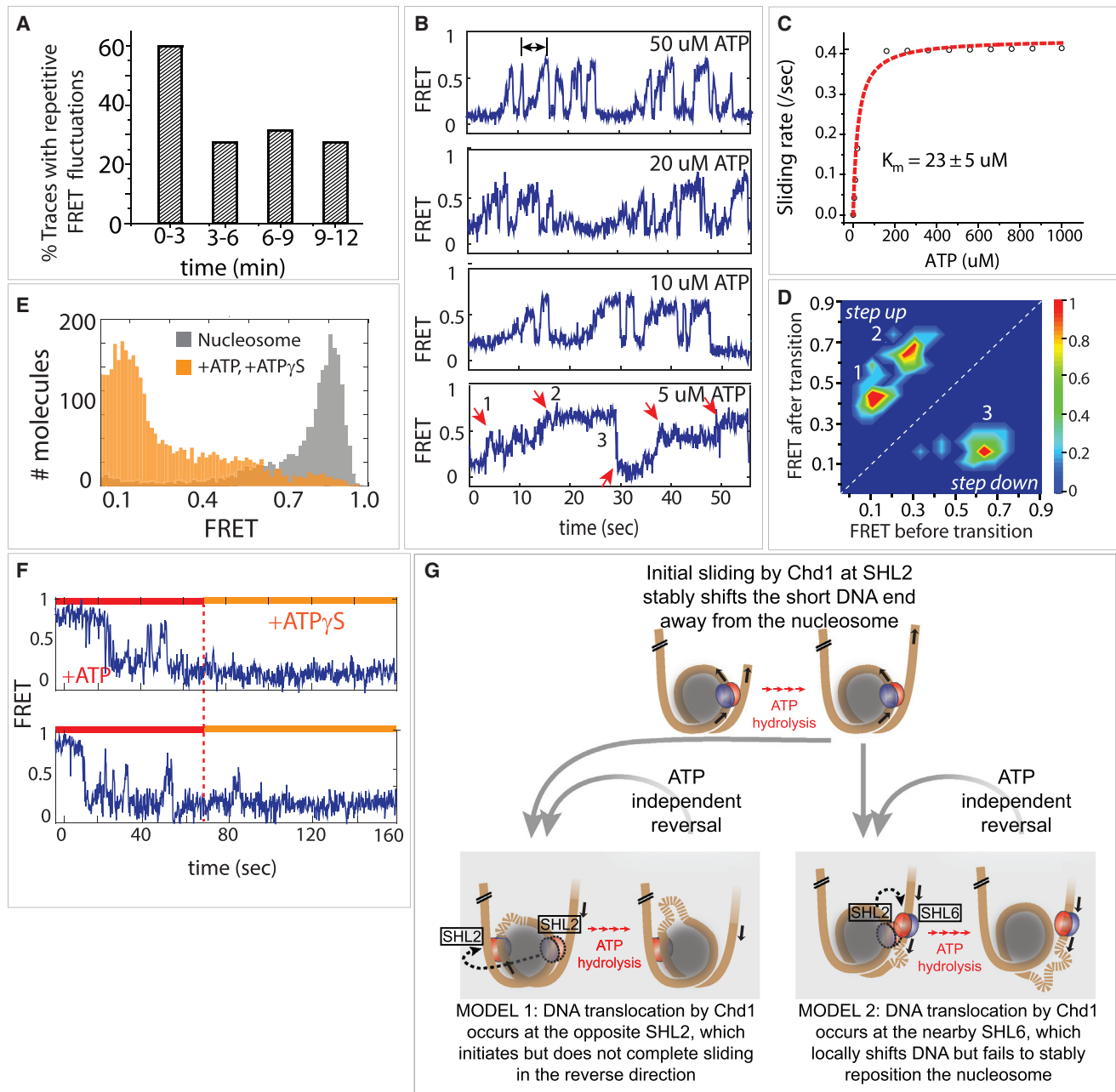


Figure 3. Repetitive Sliding Reveals an Unstable Intermediate during Remodeling

(A) Percent of traces ($n = 2,000$) showing repetitive FRET fluctuations over time.

(B) Single-molecule FRET traces taken at various ATP concentrations.

(C) Michaelis-Menten fit of repetitive FRET fluctuations.

(D) Transition density plot showing distinct FRET states visited during the repetitive movement.

(E) FRET histogram before (gray) and after addition of ATP and ATP γ S (orange).

(F) Single-molecule traces showing ATP and effect of subsequent ATP γ S addition.

(G) Two possible models to explain the bidirectional movement of nucleosomal DNA. In model 1, Chd1 changes the direction of DNA movement by engaging at the opposite SHL2, whereas in model 2, Chd1 instead engages around SHL6 located on the opposite gyre from the initial SHL2 site. In both cases, the shifted DNA is unstable without continuous ATP hydrolysis and snaps back to a remodeled state with the short DNA end away from the histone core.

23 μ M ATP and V_{\max} of $\sim 0.4/s$ (Figure 3C). We analyzed the distributions of high and low FRET levels achieved during these fluctuations by taking FRET values before and after transitions from

over 100 traces and plotting the values into a transition density plot (Figure 3D). Due to the way FRET transitions are plotted, the left top and right bottom triangles represent FRET stepping

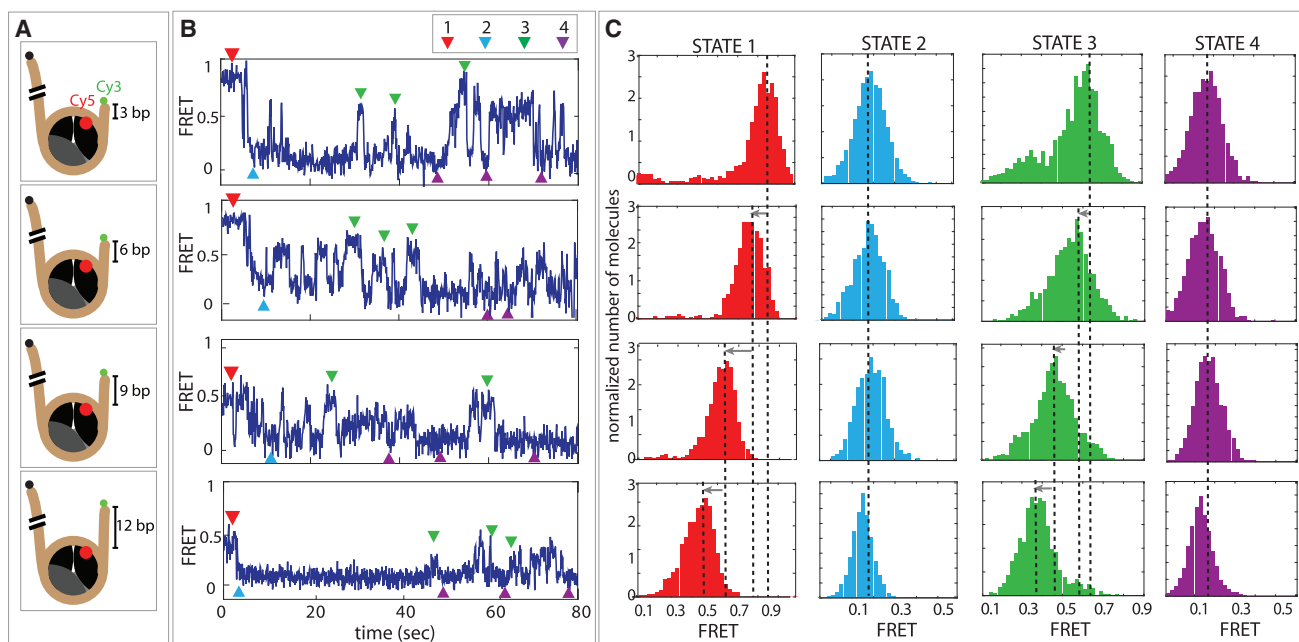


Figure 4. For the Direction of Nucleosome Sliding by Chd1, DNA Sequence Can Dominate Over the Length of Flanking DNA

(A) Schematic diagrams of four FRET-labeled nucleosome constructs with varying lengths of flanking DNA.

(B) Representative single-molecule FRET traces obtained for each nucleosome construct.

(C) FRET histograms of four distinct states: starting nucleosome position (state 1, red), short DNA end shifted away from nucleosome (state 2, light blue), short DNA end pulled back toward nucleosome (state 3, green), and repetitive low-FRET state where DNA is more distant from nucleosome (state 4, purple).

up and down, respectively. As shown, FRET steps up from 0.1 to 0.4 and 0.4 to 0.7 followed by stepping down from 0.7 to 0.1.

Although the gradual increase in FRET was consistent with Chd1 pulling the short DNA end back toward the histone core, the sudden ATP-independent drop suggested that the positioning of DNA was not stable. We hypothesized that, when Chd1 switched the direction of DNA movement, correlating with increasing FRET, ATP hydrolysis was not only required for DNA movement but also for maintaining the DNA end closer to the nucleosome. To test this notion, we initiated sliding reactions with 1 mM ATP and then introduced 1 mM ATP γ S one minute later, while the nucleosomes were undergoing back and forth motion. With this subsequent addition of ATP γ S, which removed all residual ATP, the repetitive FRET fluctuations ceased. Importantly, all molecules transitioned to the low FRET value instead of stalling at different FRET states (Figures 3E and 3F), suggesting that the higher FRET states (0.7 FRET) were unstable intermediates. We therefore conclude that ATP hydrolysis was necessary to both achieve and maintain these higher FRET states. As described in the Discussion, this behavior suggests that Chd1 pulled DNA onto the nucleosome, perhaps forming a loop or an alternative structure, which was unable to be propagated around the histone core to allow for stable repositioning (Figure 3G).

The Landscape for Chromatin Remodeling by Chd1 Is Impacted by Strong Nucleosome-Positioning Sequences

Previous work has highlighted how Chd1 preferentially shifts mononucleosomes away from DNA ends (McKnight et al.,

2011; Stockdale et al., 2006). Consistent with those findings, our single molecule fluorescence resonance energy transfer (smFRET) experiments indicate that Chd1 can shift the histone octamer away from the short DNA end of 3N80 nucleosomes and is unable to stably reposition the nucleosome back toward the short end. A basic question is therefore how Chd1 might be able to distinguish between the two sides of the nucleosome based on flanking DNA. Acting at SHL2, the remodeler ATPase motor pulls DNA onto the nucleosome from one side (entry DNA), which results in DNA being pushed onto the other side (exit DNA). Initially, movement of 3N80 nucleosomes toward the 80-bp side means that this longer flanking DNA is the entry DNA and the shorter 3-bp side is the exit side. With the subsequent reversal in sliding direction, the shorter flanking DNA becomes the entry side.

One possible explanation for preferential sliding onto the 80-bp side was that shifting nucleosomes toward the short side was inefficient due to the limited length of flanking DNA. To explore this possibility, we tested sliding for a set of nucleosomes with increasing DNA lengths on the shorter side (Figure 4A). As expected from the farther initial placement of the Cy3 donor on the short flanking DNA (6–12 bp), the initial FRET values for these nucleosomes were progressively lower. Upon addition of Chd1 and ATP, FRET values initially decreased, indicating movement in the same direction, with the Cy3-DNA end as exit DNA. As previously observed for 3N80 nucleosomes, all nucleosomes displayed FRET fluctuations suggestive of sliding in the opposite direction, yet the majority of these traces failed to achieve higher FRET than the starting values (Figure 4B).

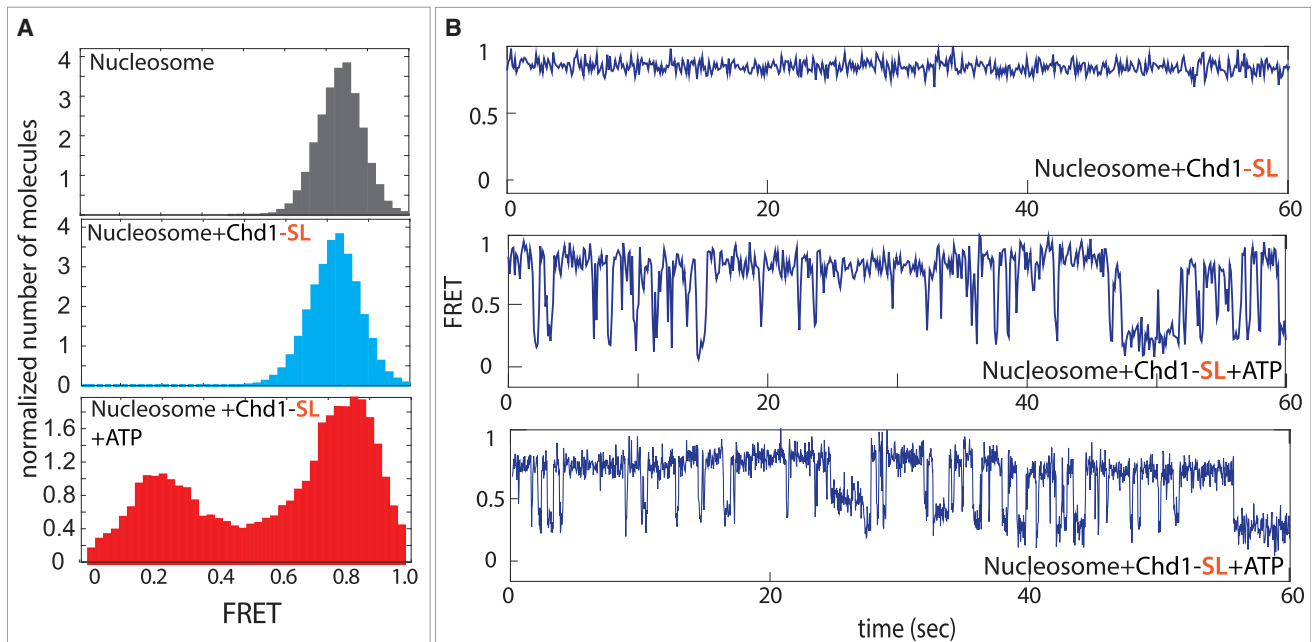


Figure 5. Restricting the DBD to Exit DNA Results in Unstable Remodeling Intermediates

(A) FRET histograms taken for nucleosome alone (gray) and nucleosomes with Chd1-SL before (light blue) and after addition of ATP (red). (B) Single-molecule traces for nucleosome and Chd1-SL without (top) and with ATP (middle and bottom).

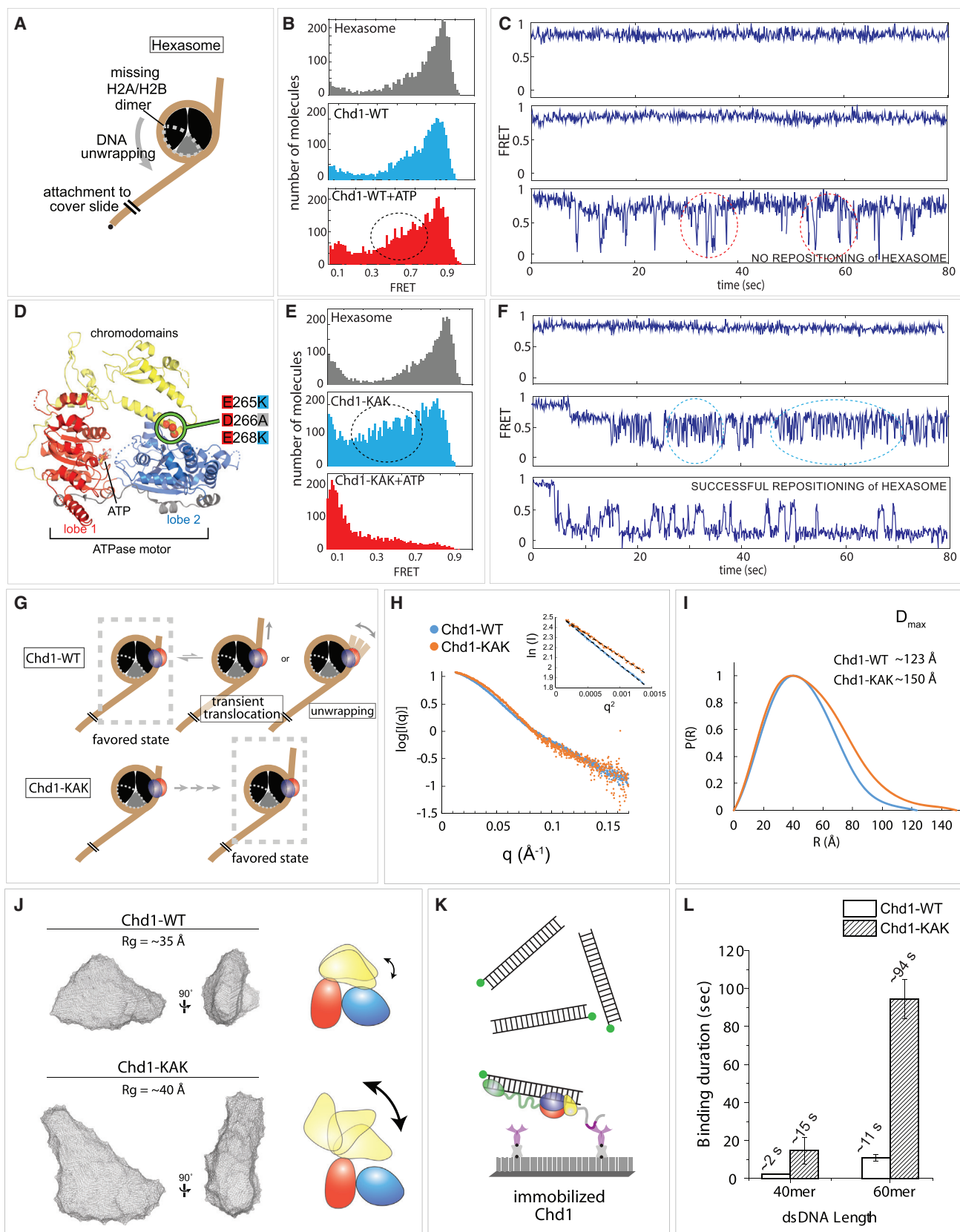
These results suggest that, despite the longer flanking DNA available for 6-, 9-, and 12-bp constructs, sliding stalled at approximately the same locations with respect to the Widom 601 positioning sequence (Figure 4C). This behavior suggests that, for these nucleosomes, the DNA sequence and not length of flanking DNA was the major determinant for the locations where remodeling intermediates were unstable.

All of the nucleosomes described so far were generated using the Widom 601 positioning sequence, and one concern was that the apparent instability of remodeling intermediates may be particular to this DNA sequence. We therefore made two additional nucleosomes (4N80 and 80N4) based on the 603 positioning sequence, which was also generated by Widom (Lowary and Widom, 1998) but shares only 28% sequence identity with 601 (Figure S1A). The 603 nucleosome showed similar smFRET patterns, shifting the short DNA end away from the nucleosome core, followed by periodic increases and decreases in FRET (Figure S1). As for 601, the FRET fluctuations were asymmetric, with slower increases in FRET compared to faster FRET decreases (Figure S1). These results support the conclusion that unstable remodeling intermediates are not unique for 601 nucleosomes. Because both 601 and 603 are strong positioning sequences, however, the high affinity for the histone core may be a major factor that destabilized remodeling intermediates in these experiments.

Limiting the Range of the Chd1 DBD Interferes with Nucleosome Sliding

The DBD of *S. cerevisiae* Chd1 is attached to the rest of the remodeler via an intrinsically disordered linker segment. We previously showed that, whereas ≤ 29 residue deletions within the

region spanning residues 961–1,005 were well tolerated, removal of the entire 45-residue stretch abrogated sliding activity (Nodelman and Bowman, 2013). Despite virtually no nucleosome sliding activity, this variant lacking residues 961–1,005, which we call Chd1-SL (for short linker), still displayed significant nucleosome-stimulated ATPase activity, suggesting that the remodeler initially engaged with nucleosomes but was unable to productively couple hydrolysis with sliding (Nodelman and Bowman, 2013). Based on the model for exit side inhibition, one explanation for the inability of Chd1-SL to slide nucleosomes could be from the persistent presence of the DBD on the exit side of the nucleosome, which is closer to SHL2, where the ATPase motor acts. Strikingly, when we tested nucleosome sliding activity of Chd1-SL by smFRET, we observed that the addition of ATP promoted an intermediate FRET state centered around 0.2 that was distinct from the fully repositioned state (0.1 FRET) described above (Figures 5A and 5B). Single-molecule traces revealed that Chd1-SL and ATP induced dynamic DNA movement without stably attaining the lowest FRET state (Figure 5B). Overall, the FRET values shifted between 0.9 and 0.2 with intermittent excursions to other mid-FRET states, which were responsible for the two broad peaks observed in Figure 5A. When Chd1-SL was added to nucleosomes in the presence of adenylyl-imidodiphosphate (AMP-PNP), remodeler-dependent FRET fluctuations were not observed (Figure S2), suggesting that ATP hydrolysis was required for altering the position of nucleosomal DNA. These results demonstrate that Chd1-SL binds and can alter the DNA organization of nucleosomes in an ATP-dependent fashion yet is somehow incapable of stably shifting DNA relative to the histone core. We speculate that this behavior reflects inhibitory action of the DBD on the nucleosome



(legend on next page)

sliding process, amplified by the shortened linker. Whereas the normal linker allows the DBD to sample both entry and exit DNA, we surmise that the shortened linker restricts the DBD to exit DNA, where it interferes with nucleosome sliding, even with limited DNA flanking the nucleosome.

The N-Terminal Chromodomains of Chd1 Guard against Sliding Hexasomes

Given the sensitivity of smFRET for detecting transient DNA movements, we decided to investigate the impact of Chd1 action on hexasomes. Compared to nucleosomes, hexasomes lack one histone H2A/H2B dimer, and we recently demonstrated that Chd1 was unable to robustly shift hexasomes toward the side lacking H2A/H2B (Levendosky et al., 2016). To monitor Chd1 activity on poor hexasome substrates, we produced end-positioned hexasomes with the side lacking the H2A/H2B dimer adjacent to the long flanking DNA, such that the Cy3-labeled DNA end was on the side with the remaining H2A/H2B dimer (Figure 6A). As expected, these hexasomes yielded a high FRET peak similar to nucleosomes (Figure 6B, top). With the absence of one H2A/H2B dimer, DNA wrapping of hexasomes appears to be weaker than that of nucleosomes, increasing the breadth of the histogram (Figure 1B). We confirmed that hexasomes engage with Chd1 in the absence of ATP by capturing FRET-labeled hexasomes with surface-immobilized Chd1 (Figure S3). Consistent with poor sliding of hexasomes, the FRET histogram in the presence of Chd1 and ATP showed only modest differences from hexasomes alone, with only a small increase in lower FRET populations (Figure 6B, bottom). Inspection of individual FRET traces, however, revealed large repetitive FRET fluctuations (Figure 6C). These dynamic FRET fluctuations were ATP dependent, and the lower FRET states were visited only transiently, rapidly reverting to the initial high-FRET state. These data are in accord with the bulk observations of poor hexasome sliding yet reveal an unexpected activity of Chd1 toward hexasomes. Rather than having a mechanistic defect in hexasome sliding, we suspected that the inability to stably maintain shifted positions reflected a dominant regulatory process that prevented the normal progression of the remodeling cycle.

In previous work, we found that disruption of the chromo-ATPase interface allowed naked DNA to activate the Chd1 ATPase similarly to nucleosomes, suggesting a loss in nucleo-

some-specific recognition (Hauk et al., 2010). Given the dynamic FRET profile of hexasomes, we wondered whether autoregulation by the chromodomains might contribute to the poor sliding of hexasomes. To investigate this possibility, we performed single-molecule sliding experiments with a Chd1 variant containing three mutations at the chromo-ATPase interface (E265K/D266A/E268K), which we refer to as Chd1-KAK (Figure 6D). On nucleosomes, remodeling by Chd1-KAK closely resembled wild-type Chd1, with characteristic ATP-dependent steps (Figure S4). On hexasome substrates, Chd1-KAK unexpectedly yielded rapid FRET fluctuations in an ATP-independent manner (Figures 6E and 6F, middle panels). Previous work from many labs has shown that DNA sliding by remodelers requires ATP hydrolysis, and therefore, we believe that the magnitude of FRET fluctuations we observed is most easily explained as dynamic DNA unwrapping from the Cy3 side of the hexasome. Interestingly, the Owen-Hughes group has reported that Chd1 can unwrap nucleosomes in the presence of AMP-PNP (Sundaramoorthy et al., 2017). In our experiments, Chd1-KAK stimulated FRET fluctuations in the absence of nucleotide, yet for wild-type Chd1, we failed to observe significant FRET fluctuations of hexasomes even with AMP-PNP (Figure S5). One possible explanation for the reported differences in 601 unwrapping for wild-type Chd1 could stem from the intrinsic asymmetry of the 601, which unwraps more readily from the one side than the other (Ngo et al., 2015). Here, we only monitored the more tightly wrapped TA-rich side of the nucleosomes, whereas Sundaramoorthy et al. (2017) followed the TA-poor side that more easily unwraps.

Unlike wild-type Chd1, upon addition of ATP, Chd1-KAK dramatically reduced FRET levels of hexasomes (Figure 6E, lower panel), suggestive of bona fide sliding. Individual smFRET traces showed a FRET decrease followed by repetitive FRET fluctuations, analogous to wild-type Chd1 with nucleosomes (Figures 6E and 6F, lower panels). To confirm that hexasomes were repositioned by Chd1-KAK, we performed histone-mapping experiments, which reveal histone locations on DNA before and after exposure to Chd1 and ATP. As shown in Figure S6, Chd1-KAK was capable of redistributing hexasomes, whereas wild-type Chd1 was not. It is not clear whether the ATP-dependent FRET fluctuations for wild-type Chd1 represent DNA unwrapping or transient DNA translocations past the histone core (Figure 6G). Regardless of the effect, these

Figure 6. Chromodomains Prevent Chd1 from Repositioning a Hexasome

- (A) Schematic diagram of hexasome conformation with the dotted gray outline indicating the location of the missing H2A-H2B dimer.
 (B) FRET histograms of hexasome alone (gray) and hexasomes plus Chd1 before (light blue) and after ATP addition (red).
 (C) Single-molecule FRET traces corresponding with conditions in (B).
 (D) Crystal structure of the chromodomain-ATPase portion of Chd1 (Hauk et al., 2010), highlighting the location of KAK mutation at the chromo-ATPase interface.
 (E) FRET histograms of hexasome alone and hexasomes plus Chd1-KAK mutant before and after ATP addition.
 (F) Single-molecule traces corresponding with conditions in (E).
 (G) Interpretations of wild-type Chd1 and Chd1-KAK mutant activities on hexasomes.
 (H) Small-angle X-ray scattering (SAXS) profiles for Chd1-wild-type (WT) and Chd1-KAK proteins consisting of just the chromodomain and ATPase motor. Guinier plot analysis (inset) shows that samples were free from aggregation.
 (I) P(R) distributions for SAXS data shown in (H).
 (J) Ab initio bead models generated by DAMMIN. Cartoons on the right illustrate possible structural changes associated with the KAK mutation.
 (K) Schematic of experiment in which Cy3-labeled dsDNA (40 or 60 bp) was added to surface-immobilized Chd1-WT or Chd1-KAK proteins. Note that these constructs contain the DBD.
 (L) Binding duration for dsDNA to both proteins (n = 500 binding events).

experiments support that wild-type Chd1 cannot effectively reposition hexasomes. Thus, disruption of chromodomain autoinhibition in Chd1-KAK allowed Chd1 to reposition hexasomes, revealing that nucleosome specificity is achieved by the ability of the chromodomains to interrupt the remodeling reaction.

Disruption of the Inhibitory Chromodomain-ATPase Interface Results in a More Extended Conformation of Chd1 and More Stable Binding to Naked DNA

What property of Chd1-KAK enables proficient repositioning of a hexasome? We hypothesized that the disruption of the chromo-ATPase interface with the KAK substitutions altered the ability of the chromodomains to stably pack against the ATPase motor and thereby reduce autoinhibition. To investigate this idea, we collected small-angle X-ray scattering (SAXS) profiles for the chromo-ATPase portion of Chd1, equivalent to that used in the crystal structure (Figure 6D). Both wild-type and KAK variants were well behaved, with low-angle scattering demonstrating that the samples were free from aggregation (Figure 6H). Consistent with the KAK substitutions weakening interdomain interactions, Chd1-KAK possessed a significantly larger radius of gyration (R_g) of $39.8 \pm 0.1 \text{ \AA}$ compared with an R_g for the wild-type chromo-ATPase of $35.6 \pm 0.1 \text{ \AA}$. The D_{\max} of the KAK mutant was also larger than wild-type (150 versus 123 \AA), indicating that disrupting this interaction between the chromodomains and ATPase motor results in a more extended conformation of the protein (Figure 6I). An extended conformation for KAK mutant was also supported by bead modeling, which suggested much looser domain-domain contacts in the absence of the wild-type chromo-ATPase interface (Figure 6J). Interestingly, whereas bead models of the wild-type chromo-ATPase showed a better fit to the crystal structure, the SAXS-derived models did not perfectly fit the shape of the chromo-ATPase crystal structure. This mismatch likely reflects dynamics of protein domains in solution that cannot be accurately represented with a static bead model. We believe that the SAXS models indicate inherent mobility of the chromodomains that are greatly exaggerated upon disruption of the chromo-ATPase interface.

One prediction of a more opened domain organization is that the ATPase motor of the KAK mutant should be able to engage more stably with DNA because the chromo-ATPase interface is disrupted. We previously reported that the KAK substitution enabled the isolated chromodomain-ATPase portion of Chd1 to weakly interact with DNA (Hauk et al., 2010); however, more recent experiments showed that the weak binding suggested by a gel shift was likely due to a contaminating factor, which could have reached significant levels relative to the 25 nM DNA probe, given the high (110 μM) concentrations of Chd1 used. Detecting DNA binding by native gel shifts is therefore not sensitive enough to reveal DNA-binding interference by the chromodomains, because the isolated chromo-ATPase does not form a stable complex with naked DNA and inclusion of the DBD masks contributions from the chromo-ATPase. We therefore turned to single-molecule observation to determine the extent that DNA binding was affected by disruption of the chromo-ATPase interface. Using Chd1 constructs containing the DBD, we tethered wild-type and KAK mutant proteins to the surface via a FLAG:anti-FLAG attachment. The protein

molecules of Chd1 were seeded at single-molecule density to which Cy3-labeled double-stranded (ds) DNA of 40 and 60 bp were added (Figure 6K). Nonspecific binding of DNA was minimal, as almost no fluorescent spots appeared when 1 nM Cy3 dsDNA was added to surface without the protein. To assess the stability of wild-type Chd1 and Chd1-KAK for binding naked dsDNA, we measured the dwell time of the Cy3 signal, which signifies the duration that dsDNA bound to the surface-immobilized protein. As shown in Figure 6L, the KAK mutant had approximately 7- to 8-fold longer retention time with 40 and 60 bp dsDNA, respectively. In addition, the KAK mutant displayed a higher apparent affinity to dsDNA compared with wild-type Chd1 (Figure S7). This higher stability of the KAK mutant with naked DNA is consistent with a more opened organization of the chromodomains that provides the ATPase motor with greater access to DNA. Given the marked gain of the KAK mutant for binding DNA and sliding hexasomes, we propose that the chromodomains are poised to disrupt interactions between the ATPase motor and nucleosomal DNA, which in turn determines how productively the remodeler engages with its nucleosome substrates.

DISCUSSION

This work advances our understanding of the Chd1 chromatin remodeler and puts forward several concepts that may also apply to other remodeling enzymes. We demonstrate that Chd1 shifts nucleosomes in predictable steps that likely encompass multiple base pairs. This behavior is consistent with the stepwise translocation observed for the related but distinct ISWI family of chromatin remodelers (Deindl et al., 2013). For ISWI, individual 1-bp steps were clustered in bursts of ~ 3 - or ~ 7 -bp steps, with pauses delineating discrete units of translocation. Interestingly, discrete multi-base-pair steps were not observed for the SWI/SNF-type remodeler remodeling of the structure of chromatin (RSC), which continuously shifted DNA using a 1- to 2-bp step size (Harada et al., 2016). The characteristic pauses that punctuate smFRET sliding patterns of Chd1 and ISWI remodelers are therefore not essential for nucleosome repositioning. We propose that these pauses provide opportunities for regulatory domains to influence the remodeling reaction. For Chd1, the N-terminal chromodomains and C-terminal DBD have both been shown to influence the remodeling reaction, and these domains may take advantage of unstable intermediate states to regulate nucleosome sliding.

Previous work with DNA gaps demonstrated that the ATPase motors of Chd1, ISWI, and SWI/SNF-type remodelers drive nucleosome repositioning by translocating on nucleosomal DNA at SHL2 (McKnight et al., 2011; Saha et al., 2005; Schwanbeck et al., 2004; Zofall et al., 2006). The ATP-dependent chromatin assembly and remodeling factor (ACF), an ISWI-type remodeler, ensures back-and-forth sliding by cooperatively binding to nucleosomes as dimers, with each remodeler ATPase poised at an SHL2 site (Racki et al., 2009). Whereas the nucleosome can simultaneously accommodate two Chd1 proteins, one at each SHL2 site (Nodelman et al., 2017), here, we make the unexpected discovery that back-and-forth movement of nucleosomal DNA can be achieved by a single Chd1

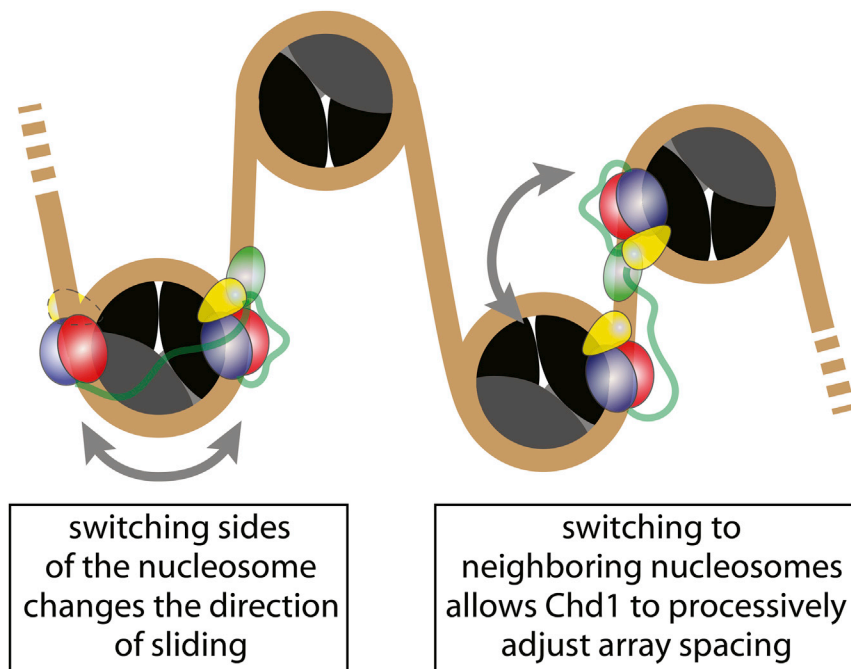


Figure 7. Proposed Model of Chd1 Generating Back and Forth Motion to Adjust Nucleosomal Spacing

of histone-histone and histone-DNA contacts, and we speculate that such repetitive remodeling events may facilitate these dramatic and fundamental reorganizations of the nucleosome.

Although the present data are insufficient for determining whether Chd1 engages with SHL6 or only switches between both SHL2 sites, the ability of the ATPase motor to sample different segments of nucleosomal DNA likely arises from flexible tethering by the DBD. The ATPase motor and DBD of Chd1 are separated by a flexible protein segment (Nodelman and Bowman, 2013) that is long enough to allow the ATPase motor to bind to SHL2 while the DBD is bound to flanking DNA on either side of the nucleosome. We propose that the

remodeler (Figure 2). After initially shifting the nucleosome away from the short end, however, Chd1 appears unable to stably shift nucleosomes in the reverse direction (Figures 3 and S1). The reason for this instability is unclear but was observed with two different positioning sequences. Whereas present evidence suggests that Chd1 shifts nucleosomes when at SHL2 (Nodelman et al., 2017), two recent studies have shown that remodeler ATPases can also engage with the outer gyre of DNA: the isolated SWI/SNF ATPase, in a cryoEM study, was shown to bind SHL6 as well as SHL2 (Liu et al., 2017) and yeast INO80 was shown to reposition nucleosomes by translocating on DNA around SHL5 (Brahma et al., 2017). For Chd1, reversal of DNA movement may therefore result from translocation of the ATPase at the SHL2 site on the opposite side of the nucleosome (Figure 3G, model 1) or by reorienting to SHL5 or SHL6 on the opposite gyre, which is close to the first SHL2 site (Figure 3G, model 2).

We speculate that the generation of unstable remodeling intermediates provides an important regulatory checkpoint. For both 601 and 603 nucleosomes, Chd1 appeared unable to stably shift nucleosomes back to the starting position, exhibiting a highly repetitive sliding behavior (Figures 3 and S1). Whereas this repetitive sliding may have been exacerbated by the absence of a C-terminal Chd1 domain of unknown function (Mohanty et al., 2016) that was absent in our construct, we note that many helicases translocate on nucleic acids in a highly repetitive manner (Koh et al., 2014; Myong et al., 2005, 2007, 2009; Myong and Ha, 2010; Park et al., 2010; Qiu et al., 2013; Tippiana et al., 2016). Analogous to keeping nucleic acids unwound, repetitive sliding by Chd1 may keep nucleosomes in alternative states. Chd1 is required for both histone replacement (Konev et al., 2007) and nucleosome assembly (Fei et al., 2015), processes that necessitate transient disruptions

ATPase motor and DBD assist each other in nucleosome binding, keeping the remodeler close to its substrate. By being tethered to the nucleosome through one domain, the high effective concentration increases the likelihood that the other domain will re-engage and also offers the possibility to sample other locations on the nucleosome. In addition to changing the direction of sliding, changes in Chd1 domain organization is also expected to affect activity. Our experiments with the shortened linker between the DBD and ATPase motor (Chd1-SL) supports an inhibitory role of the DBD on exit DNA. A shortened linker would favor a close association of the DBD and ATPase motor on opposite DNA gyres. The Chd1-SL variant shows continuous FRET fluctuations, suggestive of DNA movement, yet was unable to attain a low-FRET state, indicative of stable nucleosome repositioning (Figure 5). These results suggest that, when the DBD remains close to the ATPase motor, the nucleosome sliding reaction can be interrupted, making repositioning ineffective. The location of the ATPase motor therefore determines the direction of productive nucleosome sliding, whereas placement of the DBD relative to the ATPase motor modulates sliding activity.

We note that, although our experiments described here were limited to mononucleosomes, the dynamic re-engagement of the remodeler suggests an ability to diffuse along chromatin fibers. In a fiber, neighboring nucleosomes share the same segment of flanking DNA, and tethering by the DBD would be expected to allow the ATPase motor to also transfer to another nucleosome. In our experiments, we found a remarkably high retention of Chd1 on single nucleosomes over >20 min periods. Because monomers of Chd1 immobilized to the surface exhibited repetitive movement, the continuous Chd1 activity suggested a preference for retention on nucleosomes over dissociation into solution. These observations raise the possibility that Chd1 primarily migrates along chromatin fibers (Figure 7),

potentially also switching between fibers with close nucleosomes packing. Such a behavior would likely allow individual Chd1 remodelers to processively reorganize nucleosome positioning at a local level.

STAR★METHODS

Detailed methods are provided in the online version of this paper and include the following:

- [KEY RESOURCES TABLE](#)
- [CONTACT FOR REAGENT AND RESOURCE SHARING](#)
- [METHOD DETAILS](#)
 - Preparation and Bulk Measurements of Nucleosomes and Chd1 Proteins
 - Nucleosome and Hexasome Reconstitution and Purification
 - Single Molecule Measurements of Nucleosomes and Chd1 Proteins
- [QUANTIFICATION AND STATISTICAL ANALYSES](#)
 - For dwell time analyses
 - For initial rate analyses
 - For dsDNA binding analysis
- [DATA AND SOFTWARE AVAILABILITY](#)

SUPPLEMENTAL INFORMATION

Supplemental Information includes seven figures and one table and can be found with this article online at <http://dx.doi.org/10.1016/j.molcel.2017.08.018>.

AUTHOR CONTRIBUTIONS

Y.Q. performed all single-molecule experiments and analyzed data; R.F.L. generated nucleosome and Chd1 reagents, performed histone mapping experiments, and analyzed data; S.C. collected and analyzed SAXS data; A.P. produced nucleosome and Chd1 reagents; and G.D.B. and S.M. conceived of the project, supervised experiments, analyzed data, and wrote the paper with input from all authors.

ACKNOWLEDGMENTS

Ilana Nodelman prepared the 603 nucleosomes (4N80) and Chd1-SL protein used in this work. The authors thank members of Myong and Bowman labs and Taekjip Ha's lab for helpful discussions. This work was supported by the Human Frontier Science Program (RGP0007/2012), American Cancer Society RSG-12-066-01-DMC, NIH 1DP2GM105453, and National Science Foundation and Physics Frontiers Center Program (0822613) through the Center for the Physics of Living Cells to Y.Q. and S.M. and NIH R01-GM084192 to G.D.B.

Received: March 29, 2017

Revised: June 30, 2017

Accepted: August 18, 2017

Published: September 21, 2017

REFERENCES

- Brahma, S., Udugama, M.I., Kim, J., Hada, A., Bhardwaj, S.K., Hailu, S.G., Lee, T.H., and Bartholomew, B. (2017). INO80 exchanges H2A.Z for H2A by translocating on DNA proximal to histone dimers. *Nat. Commun.* **8**, 15616.
- Burkhardt, L., Fuchs, S., Krohn, A., Masser, S., Mader, M., Kluth, M., Bachmann, F., Huland, H., Steuber, T., Graefen, M., et al. (2013). CHD1 is a 5q21 tumor suppressor required for ERG rearrangement in prostate cancer. *Cancer Res.* **73**, 2795–2805.
- Dechassa, M.L., Sabri, A., Pondugula, S., Kassabov, S.R., Chatterjee, N., Kladde, M.P., and Bartholomew, B. (2010). SWI/SNF has intrinsic nucleosome disassembly activity that is dependent on adjacent nucleosomes. *Mol. Cell* **38**, 590–602.
- Deindl, S., Hwang, W.L., Hota, S.K., Blosser, T.R., Prasad, P., Bartholomew, B., and Zhuang, X. (2013). ISWI remodelers slide nucleosomes with coordinated multi-base-pair entry steps and single-base-pair exit steps. *Cell* **152**, 442–452.
- Dyer, P.N., Edayathumangalam, R.S., White, C.L., Bao, Y., Chakravarthy, S., Muthurajan, U.M., and Luger, K. (2004). Reconstitution of nucleosome core particles from recombinant histones and DNA. *Methods Enzymol.* **375**, 23–44.
- Fei, J., Torigoe, S.E., Brown, C.R., Khuong, M.T., Kassavetis, G.A., Boeger, H., and Kadonaga, J.T. (2015). The prenucleosome, a stable conformational isomer of the nucleosome. *Genes Dev.* **29**, 2563–2575.
- Flanagan, J.F., Mi, L.Z., Chruszcz, M., Cymborowski, M., Clines, K.L., Kim, Y., Minor, W., Rastinejad, F., and Khorasanizadeh, S. (2005). Double chromodomains cooperate to recognize the methylated histone H3 tail. *Nature* **438**, 1181–1185.
- Franke, D., and Svergun, D.I. (2009). DAMMIF, a program for rapid ab-initio shape determination in small-angle scattering. *J Appl Crystallogr.* **42**, 342–346.
- Franke, D., Petoukhov, M.V., Konarev, P.V., Panjkovich, A., Tuukkanen, A., Mertens, H.D.T., Kikhney, A.G., Hajizadeh, N.R., Franklin, J.M., Jeffries, C.M., and Svergun, D.I. (2017). ATSAS 2.8: a comprehensive data analysis suite for small-angle scattering from macromolecular solutions. *J Appl Crystallogr.* **50**, 1212–1225.
- Gaspar-Maia, A., Alajem, A., Polesso, F., Sridharan, R., Mason, M.J., Heidersbach, A., Ramalho-Santos, J., McManus, M.T., Plath, K., Meshorer, E., and Ramalho-Santos, M. (2009). Chd1 regulates open chromatin and pluripotency of embryonic stem cells. *Nature* **460**, 863–868.
- Gkikopoulos, T., Schofield, P., Singh, V., Pinskaya, M., Mellor, J., Smolle, M., Workman, J.L., Barton, G.J., and Owen-Hughes, T. (2011). A role for Snf2-related nucleosome-spacing enzymes in genome-wide nucleosome organization. *Science* **333**, 1758–1760.
- Harada, B.T., Hwang, W.L., Deindl, S., Chatterjee, N., Bartholomew, B., and Zhuang, X. (2016). Stepwise nucleosome translocation by RSC remodeling complexes. *eLife* **5**, e10051.
- Hauk, G., McKnight, J.N., Nodelman, I.M., and Bowman, G.D. (2010). The chromodomains of the Chd1 chromatin remodeler regulate DNA access to the ATPase motor. *Mol. Cell* **39**, 711–723.
- Hwang, H., Kreig, A., Calvert, J., Lormand, J., Kwon, Y., Daley, J.M., Sung, P., Opresko, P.L., and Myong, S. (2014a). Telomeric overhang length determines structural dynamics and accessibility to telomerase and ALT-associated proteins. *Structure* **22**, 842–853.
- Hwang, H., Opresko, P., and Myong, S. (2014b). Single-molecule real-time detection of telomerase extension activity. *Sci. Rep.* **4**, 6391.
- Joo, C., and Ha, T. (2008). Single-molecule FRET with total internal reflection microscopy. In *Single-Molecule Techniques: A Laboratory Manual*, P.R. Selvin and T. Ha, eds. (Cold Spring Harbor, N.Y.: Cold Spring Harbor Laboratory Press), pp. 3–35.
- Kassabov, S.R., and Bartholomew, B. (2004). Site-directed histone-DNA contact mapping for analysis of nucleosome dynamics. *Methods Enzymol.* **375**, 193–210.
- Kelley, D.E., Stokes, D.G., and Perry, R.P. (1999). CHD1 interacts with SSRP1 and depends on both its chromodomain and its ATPase/helicase-like domain for proper association with chromatin. *Chromosoma* **108**, 10–25.
- Koh, H.R., Xing, L., Kleiman, L., and Myong, S. (2014). Repetitive RNA unwinding by RNA helicase A facilitates RNA annealing. *Nucleic Acids Res.* **42**, 8556–8564.
- Konarev, D.V., Khasanov, S.S., Saito, G., Lyubovskaya, R.N., Yoshida, Y., and Otsuka, A. (2003). The interaction of C60, C70, and C60(CN)₂ radical anions

- with cobalt(II) tetraphenylporphyrin in solid multicomponent complexes. *Chemistry* 9, 3837–3848.
- Konev, A.Y., Tribus, M., Park, S.Y., Podhraski, V., Lim, C.Y., Emelyanov, A.V., Vershilova, E., Pirrotta, V., Kadonaga, J.T., Lusser, A., and Fyodorov, D.V. (2007). CHD1 motor protein is required for deposition of histone variant H3.3 into chromatin in vivo. *Science* 317, 1087–1090.
- Krogan, N.J., Kim, M., Ahn, S.H., Zhong, G., Kobor, M.S., Cagney, G., Emili, A., Shilatifard, A., Buratowski, S., and Greenblatt, J.F. (2002). RNA polymerase II elongation factors of *Saccharomyces cerevisiae*: a targeted proteomics approach. *Mol. Cell. Biol.* 22, 6979–6992.
- Levendosky, R.F., Sabantsev, A., Deindl, S., and Bowman, G.D. (2016). The Chd1 chromatin remodeler shifts hexasomes unidirectionally. *eLife* 5, e21356.
- Li, G., and Widom, J. (2004). Nucleosomes facilitate their own invasion. *Nat. Struct. Mol. Biol.* 11, 763–769.
- Lin, J.J., Lehmann, L.W., Bonora, G., Sridharan, R., Vashisht, A.A., Tran, N., Plath, K., Wohlschlegel, J.A., and Carey, M. (2011). Mediator coordinates PIC assembly with recruitment of CHD1. *Genes Dev.* 25, 2198–2209.
- Liu, X., Li, M., Xia, X., Li, X., and Chen, Z. (2017). Mechanism of chromatin remodelling revealed by the Snf2-nucleosome structure. *Nature* 544, 440–445.
- Lowary, P.T., and Widom, J. (1998). New DNA sequence rules for high affinity binding to histone octamer and sequence-directed nucleosome positioning. *J. Mol. Biol.* 276, 19–42.
- Lusser, A., Urwin, D.L., and Kadonaga, J.T. (2005). Distinct activities of CHD1 and ACF in ATP-dependent chromatin assembly. *Nat. Struct. Mol. Biol.* 12, 160–166.
- Mathew, E., Mirza, A., and Menhart, N. (2004). Liquid-chromatography-coupled SAXS for accurate sizing of aggregating proteins. *J. Synchrotron Radiat.* 11, 314–318.
- McKnight, J.N., Jenkins, K.R., Nodelman, I.M., Escobar, T., and Bowman, G.D. (2011). Extranucleosomal DNA binding directs nucleosome sliding by Chd1. *Mol. Cell. Biol.* 31, 4746–4759.
- Mohanty, B., Helder, S., Silva, A.P., Mackay, J.P., and Ryan, D.P. (2016). The chromatin remodelling protein CHD1 contains a previously unrecognised C-terminal helical domain. *J. Mol. Biol.* 428, 4298–4314.
- Myong, S., and Ha, T. (2010). Stepwise translocation of nucleic acid motors. *Curr. Opin. Struct. Biol.* 20, 121–127.
- Myong, S., Rasnik, I., Joo, C., Lohman, T.M., and Ha, T. (2005). Repetitive shuttling of a motor protein on DNA. *Nature* 437, 1321–1325.
- Myong, S., Bruno, M.M., Pyle, A.M., and Ha, T. (2007). Spring-loaded mechanism of DNA unwinding by hepatitis C virus NS3 helicase. *Science* 317, 513–516.
- Myong, S., Cui, S., Cornish, P.V., Kirchofer, A., Gack, M.U., Jung, J.U., Hopfner, K.P., and Ha, T. (2009). Cytosolic viral sensor RIG-I is a 5'-triphosphate-dependent translocase on double-stranded RNA. *Science* 323, 1070–1074.
- Narlikar, G.J., Sundaramoorthy, R., and Owen-Hughes, T. (2013). Mechanisms and functions of ATP-dependent chromatin-remodeling enzymes. *Cell* 154, 490–503.
- Ngo, T.T., Zhang, Q., Zhou, R., Yodh, J.G., and Ha, T. (2015). Asymmetric unwrapping of nucleosomes under tension directed by DNA local flexibility. *Cell* 160, 1135–1144.
- Nodelman, I.M., and Bowman, G.D. (2013). Nucleosome sliding by Chd1 does not require rigid coupling between DNA-binding and ATPase domains. *EMBO Rep.* 14, 1098–1103.
- Nodelman, I.M., Horvath, K.C., Levendosky, R.F., Winger, J., Ren, R., Patel, A., Li, M., Wang, M.D., Roberts, E., and Bowman, G.D. (2016). The Chd1 chromatin remodeler can sense both entry and exit sides of the nucleosome. *Nucleic Acids Res.* 44, 7580–7591.
- Nodelman, I.M., Bleichert, F., Patel, A., Ren, R., Horvath, K.C., Berger, J.M., and Bowman, G.D. (2017). Interdomain communication of the Chd1 chromatin remodeler across the DNA gyres of the nucleosome. *Mol. Cell* 65, 447–459.e6.
- Park, J., Myong, S., Niedziela-Majka, A., Lee, K.S., Yu, J., Lohman, T.M., and Ha, T. (2010). PcrA helicase dismantles RecA filaments by reeling in DNA in uniform steps. *Cell* 142, 544–555.
- Patel, A., McKnight, J.N., Genzor, P., and Bowman, G.D. (2011). Identification of residues in chromodomain helicase DNA-binding protein 1 (Chd1) required for coupling ATP hydrolysis to nucleosome sliding. *J. Biol. Chem.* 286, 43984–43993.
- Patel, A., Chakravarthy, S., Morrone, S., Nodelman, I.M., McKnight, J.N., and Bowman, G.D. (2013). Decoupling nucleosome recognition from DNA binding dramatically alters the properties of the Chd1 chromatin remodeler. *Nucleic Acids Res.* 41, 1637–1648.
- Qiu, Y., and Myong, S. (2016). Single-molecule imaging with one color fluorescence. *Methods Enzymol.* 581, 33–51.
- Qiu, Y., Antony, E., Doganay, S., Koh, H.R., Lohman, T.M., and Myong, S. (2013). Srs2 prevents Rad51 filament formation by repetitive motion on DNA. *Nat. Commun.* 4, 2281.
- Racki, L.R., Yang, J.G., Naber, N., Partensky, P.D., Acevedo, A., Purcell, T.J., Cooke, R., Cheng, Y., and Narlikar, G.J. (2009). The chromatin remodeler ACF acts as a dimeric motor to space nucleosomes. *Nature* 462, 1016–1021.
- Roy, R., Hohng, S., and Ha, T. (2008). A practical guide to single-molecule FRET. *Nat. Methods* 5, 507–516.
- Saha, A., Wittmeyer, J., and Cairns, B.R. (2005). Chromatin remodeling through directional DNA translocation from an internal nucleosomal site. *Nat. Struct. Mol. Biol.* 12, 747–755.
- Schwanbeck, R., Xiao, H., and Wu, C. (2004). Spatial contacts and nucleosome step movements induced by the NURF chromatin remodeling complex. *J. Biol. Chem.* 279, 39933–39941.
- Simic, R., Lindstrom, D.L., Tran, H.G., Roinick, K.L., Costa, P.J., Johnson, A.D., Hartzog, G.A., and Arndt, K.M. (2003). Chromatin remodeling protein Chd1 interacts with transcription elongation factors and localizes to transcribed genes. *EMBO J.* 22, 1846–1856.
- Sims, R.J., 3rd, Millhouse, S., Chen, C.F., Lewis, B.A., Erdjument-Bromage, H., Tempst, P., Manley, J.L., and Reinberg, D. (2007). Recognition of trimethylated histone H3 lysine 4 facilitates the recruitment of transcription postinitiation factors and pre-mRNA splicing. *Mol. Cell* 28, 665–676.
- Smolle, M., Venkatesh, S., Gogol, M.M., Li, H., Zhang, Y., Florens, L., Washburn, M.P., and Workman, J.L. (2012). Chromatin remodelers Isw1 and Chd1 maintain chromatin structure during transcription by preventing histone exchange. *Nat. Struct. Mol. Biol.* 19, 884–892.
- Stockdale, C., Flaus, A., Ferreira, H., and Owen-Hughes, T. (2006). Analysis of nucleosome repositioning by yeast ISW1 and Chd1 chromatin remodeling complexes. *J. Biol. Chem.* 281, 16279–16288.
- Sundaramoorthy, R., Hughes, A.L., Singh, V., Wiechens, N., Ryan, D.P., El-Mkami, H., Petoukhov, M., Svergun, D.I., Treutlein, B., Quack, S., et al. (2017). Structural reorganization of the chromatin remodeling enzyme Chd1 upon engagement with nucleosomes. *eLife* 6, e22510.
- Tippiana, R., Xiao, W., and Myong, S. (2014). G-quadruplex conformation and dynamics are determined by loop length and sequence. *Nucleic Acids Res.* 42, 8106–8114.
- Tippiana, R., Hwang, H., Opresko, P.L., Bohr, V.A., and Myong, S. (2016). Single-molecule imaging reveals a common mechanism shared by G-quadruplex-resolving helicases. *Proc. Natl. Acad. Sci. USA* 113, 8448–8453.
- Volkov, V.V., and Svergun, D.I. (2003). Uniqueness of ab-initio shape determination in small-angle scattering. *J. Appl. Cryst.* 36, 860–864.
- Zhao, D., Lu, X., Wang, G., Lan, Z., Liao, W., Li, J., Liang, X., Chen, J.R., Shah, S., Shang, X., et al. (2017). Synthetic essentiality of chromatin remodelling factor CHD1 in PTEN-deficient cancer. *Nature* 542, 484–488.
- Zofall, M., Persinger, J., Kassabov, S.R., and Bartholomew, B. (2006). Chromatin remodeling by ISW2 and SWI/SNF requires DNA translocation inside the nucleosome. *Nat. Struct. Mol. Biol.* 13, 339–346.

STAR★METHODS

KEY RESOURCES TABLE

REAGENT or RESOURCE	SOURCE	IDENTIFIER
Antibodies		
Monoclonal ANTI-FLAG® BioM2 antibody produced in mouse	Sigma-Aldrich	Cat # F9291
Chemicals, Peptides, and Recombinant Proteins		
Nonidet P-40	Fisher Scientific	Cat # MP1RIST1315
BSA	New England Biolabs	Cat # B9000S
Glucose Oxidase from <i>Aspergillus niger</i> , Type VII	Sigma Aldrich	Cat # G2133
Catalase from bovine liver	Sigma Aldrich	Cat # C30
4-Azidophenacyl bromide	Sigma Aldrich	A6057
Phenol:Chloroform 5:1	Sigma Aldrich	P1944
Cy3 Mono-Reactive NHS Ester	GE Healthcare	Cat # PA13105
Cy5 maleimide	Lumiprobe	43080
Adenosine triphosphate disodium salt hydrate	Sigma Aldrich	A1852
Adenosine 5'-(β,γ -imido)triphosphate lithium salt hydrate (AMPPNP)	Sigma Aldrich	A2647
Adenosine 5'-[γ -thio]triphosphate tetralithium salt	Sigma Aldrich	A1388
Phusion DNA Polymerase	NEB	M0530
Recombinant DNA		
Chd1	McKnight et al., 2011	N/A
Chd1 SL	Nodelman and Bowman, 2013	N/A
Chd1 KAK	This paper	N/A
Chd1 FLAG	This paper	N/A
Chd1 KAK FLAG	This paper	N/A
Histone H2A	Karolin Luger Lab	N/A
Histone H2A-T120C	Geeta Narlikar Lab	N/A
Histone H2B	Karolin Luger Lab	N/A
Histone H2B-S53C	Blaine Bartholomew Lab	N/A
Histone H3-C110A	Blaine Bartholomew Lab	N/A
Histone H4	Karolin Luger Lab	N/A
pGEM 601	Jonathan Widom Lab	N/A
pGEM 601(LacO-11R)	Nodelman et al., 2016	N/A
P159 603-31-601	Dechassa et al., 2010	N/A
Software and Algorithms		
ATSAS 2.8.2 for SAXS data processing	Franke et al., 2017	https://www.embl-hamburg.de/biosaxs/software.html
PRIMUS	Konarev et al., 2003	https://www.embl-hamburg.de/biosaxs/primus.html
DAMMIF	Franke and Svergun, 2009	https://www.embl-hamburg.de/biosaxs/dammif.html
DAMAVR	Volkov and Svergun, 2003	https://www.embl-hamburg.de/biosaxs/damaver.html
DAMFILT	Volkov and Svergun, 2003	https://www.embl-hamburg.de/biosaxs/damaver.html

(Continued on next page)

Continued

REAGENT or RESOURCE	SOURCE	IDENTIFIER
smCamera	Ha Lab at JHU	https://cplc.illinois.edu/software/
IDL	Research Systems, Inc.	http://www.exelisvis.co.uk/ProductsServices/IDL.aspx
IDL scripts	Ha Lab at JHU	https://cplc.illinois.edu/software/
MATLAB	Mathworks	https://www.mathworks.com/products/matlab.html
MATLAB scripts	Ha Lab at JHU	https://cplc.illinois.edu/software/
OriginLab	OriginLab Corporation	http://www.originlab.com/
Other		
HisPrep FF 16/10 (Nickel affinity)	GE	28-9365-51
HisTrap HP, 5ml (Nickel affinity)	GE	17-5248-01
HiTrap SP FF, 5ml	GE	17-5157-01
HiTrap Q FF, 5ml	GE	17-5156-01
HiLoad 16/600 Superdex 200, prep grade	GE	28-9893-35
HiPrep 26/10 Desalting	GE	17-5087-01
HiPrep 16/10 Q FF	GE	17-5190-01
HiPrep 16/10 SP FF	GE	17-5192-01

CONTACT FOR REAGENT AND RESOURCE SHARING

Further information and requests for resources and reagents should be directed to and will be fulfilled by the Lead Contact, Sua Myong (smyong@jhu.edu).

METHOD DETAILS**Preparation and Bulk Measurements of Nucleosomes and Chd1 Proteins****Histone purification**

Histones were prepared essentially as previously described (Dyer et al., 2004). *Xenopus laevis* histones H2A, H2B, H3 and H4 were expressed in bacteria and FPLC purified. pET3a vectors containing expression constructs of each *Xenopus laevis* histone were transformed into *Escherichia coli* BL21(DE3) pLysS cells, grown at 37°C in 4 L of 2x TY media (containing ampicillin and chloramphenicol) and induced with IPTG at OD₆₀₀ = 0.3-0.5. Cells were harvested at room temperature and resuspended to ~40mL in wash buffer (50 mM Tris-HCl pH 7.5, 100 mM NaCl, 1 mM ethylenediaminetetraacetic acid (EDTA) pH 8, with 1 mM Benzamidine added fresh before use) and flash frozen in liquid nitrogen. The pellet was thawed, diluted to ~80 mL in wash buffer and sonicated. The insoluble fraction containing the histone-rich inclusion bodies was pelleted by centrifugation at 23,000 x g for 20 min at 4°C. The supernatant was discarded and the pellet was thoroughly resuspended in 80 mL of wash buffer with 1% v/v Triton X-100 detergent followed by centrifugation for 10 min. The pellet was washed once more with wash buffer plus detergent and then two more times with wash buffer. After the last wash, the inclusion body pellet was spread in a thin layer on the inside of a 50 mL conical tube and stored at -20°C. To purify the histones from the inclusion bodies, the inclusion bodies were treated with 1 mL of DMSO and incubated at room temperature for 30 min and then the histones were unfolded with 40 mL of unfolding buffer (20 mM Tris-HCl pH 7.5, 7 M guanidine-HCl, 1 mM EDTA pH 8, 10 mM DTT, prepared fresh) and shaken at room temperature for one hour. The inclusion bodies were centrifuged at 23,000x g for 20 min at 18°C and the supernatant was passed over a desalting column (HiPrep 26/10; 17-5087-01) pre-equilibrated in desalting buffer (10 mM Tris-HCl pH 7.5, 7 M Urea, 1 mM EDTA, 100 mM NaCl, 5 mM β-Mercaptoethanol, prepared fresh and degassed) 20 mL at a time to remove the guanidine-HCl. Next, the histones were loaded onto a Q anion exchange column (HiPrep 16/10 Q FF, 17-5190-01) mounted on top of an S cation exchange column (HiPrep 16/10 SP FF, 17-5192-01), which were both pre-equilibrated in ion exchange buffer A (10 mM Tris-HCl pH 7.5, 7 M Urea, 1 mM EDTA, 5 mM β-Mercaptoethanol, prepared fresh and degassed) with 10% ion exchange buffer B (ion exchange buffer A with 1 M NaCl). After loading, the tandem ion exchange columns were washed until the UV signal reached baseline. The Q column was then removed and the S column was washed further. A linear gradient from 10% to 60% ion exchange buffer B (100 mM to 600mM NaCl) over 30 column volumes was used to elute the histones from the S column. After evaluation by 18% SDS-PAGE, peak fractions were pooled and dialyzed in 3500 MWCO dialysis tubing against 4 L of 5 mM β-Mercaptoethanol with two more buffer changes with at least 3 hr between changes. The purified histones were lyophilized in 2 mg aliquots and stored at -20°C.

Refolding of histone dimer and histone tetramer

The histones were refolded into high salt buffer to form dimer (H2A/H2B) and tetramer ($[(\text{H3}/\text{H4})_2]$), which could later be combined in different ratios with DNA to form either nucleosomes or hexasomes. Each 2 mg histone aliquot was unfolded at room temperature in 1.5 mL unfolding buffer (20 mM Tris-HCl, pH 7.8, 6 M guanidine-HCl, 5 mM DTT, made fresh). After 1–2 hr, undissolved protein was removed by centrifugation at 16,100 \times g for 10 min at room temperature. The unfolded histones were combined in equimolar ratios, adjusted to a final histone concentration of 1 mg/mL and placed in 3500 MWCO dialysis tubing. The histones were dialyzed into four changes of 500 mL refolding buffer (10 mM Tris, pH 7.8, 2 M NaCl, 1 mM EDTA, 5 mM β -mercaptoethanol added fresh) at least 3 hr apart.

For FRET experiments, residue 120 of H2A was mutated to cysteine and labeled with Cy5 maleimide. Histones to be labeled were unfolded with 1.5 mL labeling buffer (20 mM Tris, pH 7.0, 6 M guanidine-HCl, 5 mM EDTA) for each 2 mg aliquot. The cysteines were reduced by adding 4 μ L of 500 mM TCEP and then the histones were incubated for 2 hr at room temperature. Each 2 mg aliquot of histone was labeled with 5 μ M of Cy5 maleimide and incubated for 3 hr at room temperature in the dark. The labeling reaction was quenched with 80 mM β -Mercaptoethanol and the unreacted dye was removed by buffer exchanging with labeling buffer using an Amicon Ultra 3,500 MWCO concentrator. The labeled histone could then be combined with the other histones and dialyzed into refolding buffer.

Dimer and tetramer were purified individually by FPLC. The dimer or tetramer was concentrated in an Amicon Ultra 10,000 MWCO concentrator to \sim 1 mL and loaded onto a HiLoad 16/10 Superdex 75 size exclusion column pre-equilibrated in degassed refolding buffer. Peak fractions were analyzed by 18% SDS-PAGE and clean fractions with equal amounts of composite histones were pooled and concentrated. The dimer or tetramer was mixed 1:1 with freezing solution (10 mM Tris, pH 7.8, 2 M NaCl, 1 mM EDTA, 5 mM β -mercaptoethanol, 40% (v/v) glycerol), flash frozen in liquid nitrogen and stored at -80°C .

Preparation of Nucleosomal DNA

(See Table S1 for a complete DNA sequence information)

DNA containing the Widom 601 or 603 nucleosome (Dechassa et al., 2010) positioning sequences were prepared by PCR in 5 or 10 mL reactions. DNA constructs were as follows (linker DNA lowercase and dyad bold/underlined):

601 (3N80), 5'cccTGGAGAATCCCGGTGCCGAGGCCGCTCAATTGGTCGTAGACAGCTCTAGCACCGCTTAAACGCACGTACGCGCTGTCCCCCGCGTTTTAACCGCCAAGGGGATTACTCCCTAGTCTCCAGGCACGTGTCAGATATATACATCCTGtgcattgattgaacgacacctgcccgggtgccagtcggatagttccgagctcccactctagaggatccccgggtaccg;

603 (4N80), 5'tgccCAGTTCGCGCGCCACCTACCGTGTGAAGTCGTCACTCGGGCTTCTAAGTACGCTTAGCGCACGGTAGAGCGCAATCCAAAGGCTAACACCGTGCATCGATGTTGAAAGGGCCCTCCGTCCTTATTACTTCAAGTCCCTGGGGtaccctgttcgaggtcgactctagaggatcccagagagaatcccgggtgccgagggccgctcaattggctgtagacagctcta;

603 (80N4), 5'cacaggaacagctatgaccatgattacgccaagctcggaggacagctcctcgtgcaggtcgactctagaggatctgccCAGTTCGCGCGCCACCTACCGTGTGAAGTCGTCACTCGGGCTTCTAAGTACGCTTAGCGCACGGTAGAGCGCAATCCAAAGGCTAACACCGTGCATCGATGTTGAAAGGGCCCTCCGTCCTTATTACTTCAAGTCCCTGGGGtaca

Reactions contained 1x ThermoPol buffer, 2 mM MgSO_4 , 2 ng/ μ L pGEM 601 plasmid, 0.5 μ M forward and reverse primers, 2 mM dNTP mixture, and Taq Polymerase. Primers containing fluorophores or biotin were ordered from IDT. The reaction was divided into 100 μ L aliquots in thin-walled PCR tubes and placed in a thermocycler programed as follows: Step 1— 95°C for 1 min, Step 2— 95°C for 30 s, Step 3— 55°C for 30 s, Step 4— 72°C for 1 min, Step 5—go to Step 2 40 times, Step 6— 72°C for 10 min. The individual aliquots were pooled and the PCR product was verified by 1.5% agarose electrophoresis with a 100 bp ladder.

Next, the target DNA was purified away from primers and incomplete products over a BioRad MiniPrep Cell apparatus. The PCR product was concentrated to \sim 50 μ L in an Amicon Ultra 4 concentrator and sucrose was added to 8%. The PCR product was loaded on a 5.5 cm tall, 6% polyacrylamide (60:1 acrylamide:bisacrylamide) native MiniPrep Cell column and electrophoresed at 1 W using 0.5 \times TBE running buffer and TE elution buffer (10 mM Tris pH 7.8, 1 mM EDTA pH 8). Elution fractions were collected at a rate of 3 min/fraction and analyzed on a 1.5% agarose gel. DNA usually eluted after about 2 hr. Clean peak fractions were pooled and concentrated before measuring the DNA concentration at A_{260} – A_{310} .

Nucleosome and Hexasome Reconstitution and Purification

The protocol for generating nucleosomes followed Dyer et al., 2004. Nucleosome and hexasome reconstitutions were assembled containing 5.95 μ M purified DNA, 2 M NaCl, 10 mM Tris pH 7.8, 1 mM EDTA pH 8, 1 mM DTT, 6 μ M $[(\text{H3}/\text{H4})_2]$ tetramer, and 12 μ M H2A/H2B dimer (to make nucleosomes) or 7.2 μ M H2A/H2B (to make hexasomes). The components were loaded into small 6–8,000 MWCO dialysis chambers and placed in 400 mL of cold, high-salt reconstitution buffer (RB high: 10 mM Tris-HCl pH 7.8, 2 M KCl, 1 mM EDTA pH 8, 1 mM DTT added fresh). The reconstitution buffer was stirred at 4°C in the dark while 2 L of a low salt buffer (RB low: same as RB high but containing 250 mM KCl) was exchanged with RB high at a rate of 1.5 mL/minute. After all of the RB low was exchanged, the reconstitution was transferred to 400 mL of TED buffer (10mM Tris-HCl pH 7.8, 1 mM EDTA pH 8, and 1 mM DTT added fresh) to dialyze for at least 3 more hours. The reconstitutions were concentrated to \sim 50 μ L and brought to 8% sucrose in preparation for purification and stored on ice at 4°C .

Nucleosome or hexasome reconstitutions were purified using a BioRad MiniPrep Cell. The column was 7 cm tall, 7% polyacrylamide (60:1 acrylamide:bisacrylamide). The samples were electrophoresed at 1 W using 0.5 \times TBE running buffer and TED elution buffer. Hexasomes usually eluted in 4.5 to 5 hr and nucleosomes eluted in 5 to 6 hr. Samples of eluted fractions were mixed

1:1 with 12% sucrose loading buffer and evaluated using 7% polyacrylamide (60:1 acrylamide:bisacrylamide) native minigels, with a 100-fold dilution of the loaded reconstitutions providing a marker. Pure fractions were pooled and concentrated to at least 2 μ M as measured by the DNA concentration. Pure nucleosome or hexasome was brought to 20% glycerol and 0.1 mg/mL BSA then flash frozen in liquid nitrogen and stored at -80°C .

Histone Mapping

The position of the histone octamer can be determined to near bp resolution using histone mapping as previously described (Kassabov and Bartholomew, 2004). Nucleosomes or hexasomes containing a single cysteine mapping site introduced at H2B (S53C) and fluorescently labeled DNA were buffer exchanged into TG buffer to remove DTT. The mapping site was labeled with 200–400 nM of the photactivatable crosslinker 4-azidophenacyl bromide (APB) at room temperature in the dark for 2.5 hr then quenched with DTT. Mapping reactions (50 μ L) were assembled with 150 nM nucleosome or hexasome and 50 nM Chd1 in 1x slide buffer (20 mM Tris-HCl (pH 7.8), 50 mM KCl, 5 mM MgCl_2 , 5% sucrose (w/v), 0.1 mg/mL BSA, 1 mM DTT). Sliding reactions were initiated with the addition of 2 mM ATP and quenched at time points by mixing with 100 μ L of quench buffer (20 mM Tris-HCl (pH 7.8), 50 mM KCl, 5% sucrose (w/v), 0.1 mg/mL BSA, 5 mM DTT, 5 mM EDTA, 150 ng/mL salmon sperm DNA) and chilled on ice. Quenched reactions were UV irradiated for 15 s to induce APB crosslinking to DNA. Irradiated samples were mixed with 150 μ L of 20 mM Tris-HCl pH 8, 0.2% SDS, 50 mM NaCl and heated to 70°C for 20 min. Next, 300 μ L of 5:1 Phenol:Chloroform was added, followed by vortexing and centrifugation at 16,100 x g for 2 min. About 250 μ L of the top layer containing un-crosslinked DNA was removed. The sample was washed by adding 280 μ L of 1M Tris-HCl pH 8 and 1% SDS and then vortexing, centrifuging, and removing 280 μ L from the top layer. This wash step was repeated three more times. DNA was precipitated by addition of 33 μ L NaAcetate pH 5.2, 1.5 μ L salmon sperm DNA and 750 μ L of 100% EtOH. Samples were mixed and stored on ice at 4°C overnight. Precipitated DNA was pelleted by centrifugation at 16,100 x g for 30 min at 4°C and the supernatant was discarded. The pellet was washed with 750 μ L of 75% EtOH two times then allowed to dry. The DNA pellet was resuspended by adding 100 μ L Ammonium Acetate, 2% SDS, 1mM EDTA pH 8, and vortexing for 1 min. The DNA was cleaved at the crosslinking site through the addition of 5 μ L NaOH and heating at 90°C for 40 min. The samples were neutralized with the addition of 105 μ L of 20 mM Tris-HCl and 6 μ L of 2 M HCl and vortexed. The cleaved DNA was precipitated with the addition of 1 μ L 2M MgCl_2 and 480 μ L 100% EtOH, and incubated at -20°C overnight. The precipitated DNA was pelleted, washed, and dried as before. The dry pellet was resuspended in 4 μ L of deionized formamide loading buffer (89 mM Tris-borate pH 8, 5 mM EDTA pH 8, 95% (v/v) formamide, 0.2% (w/v) Orange G Dye). For reference, a sequencing ladder was prepared using USB-Affymetrix Thermo Sequenase Dye Primer Manual Cycle Sequencing Kit (cat# 79260) with the labeled primer used to generate the nucleosomal DNA. Sequencing reactions were mixed 1:1 with formamide loading buffer and heated to 70°C for 2 min. The mapping samples were heated at 95°C for ~ 30 s before loading on an 8% polyacrylamide (19:1 acrylamide:bisacrylamide) 7.7 M urea sequencing gel alongside the sequencing ladder. The gel was run for 1.25 hr at 65 W using 1x TBE running buffer and visualized on a Typhoon 9410 variable mode imager (GE Healthcare).

Chd1 protein purification

A truncated construct of *Saccharomyces cerevisiae* Chd1 (residues 118–1274), here referred to simply as Chd1, was purified as previously described (Nodelman et al., 2017; Patel et al., 2011). All Chd1 expression constructs contained an N-terminal 6 X His tag followed by a PreScission Protease cut site (LEVLFQ/GP). The N-termini of FLAG tag constructs were as follows (pre-scission cleavage site bolded, and FLAG tags underlined; final D in sequence is residue 175): MSYYHHHHHLESTSLYKKGSAAPFT **GSLEVLFQGP**QSTVKIPTRFSNRQNKTVNYNIDYSDDDLLESEDDYKDDDDKGSEALSDLLESEDDYKDDDDKGSEALSEENVHEAS ANPQPED. FLAG tagged constructs also lacked any with endogenous cysteines and contained two introduced cysteines at positions Q255C and K632C, which showed remodeling activity comparable to wild-type Chd1. The Chd1 KAK mutant contained amino acid changes E265K, D266A, and E268K. Chd1-SL additionally contained an internal deletion of residues 961–1005 (Nodelman and Bowman, 2013)

Each expression construct, in a pDEST17 vector, was transformed into chemically competent *Escherichia coli* BL21(DE3) Trigger RIL cells for expression, plated on LB agar plates containing ampicillin (to retain pDEST17) and chloramphenicol (to retain the Trigger RIL plasmid). Overnight cultures started from single colonies were used to inoculate eight 1 L cultures of TB media containing ampicillin and chloramphenicol in baffled Fernbach flasks, and grown at 37°C . Once the expression cultures reached $\text{OD}_{600} = 0.2\text{--}0.4$, the temperature of the incubator was reduced to 18°C . At $\text{OD}_{600} = 0.6\text{--}0.8$, Chd1 expression was induced by the addition of 0.3 mM IPTG and the cultures were incubated for an additional 18 hr. Cells were harvested by centrifugation at 4000 x g for 10 min at 4°C . Cell pellets were flash frozen in liquid nitrogen and stored at -80°C .

The Chd1 proteins were FPLC purified. Cell pellets were thawed in room temperature water bath and immediately placed on ice. Pellets were resuspended in HisBind Buffer A (20mM Tris-HCl pH 7.8, 500 mM NaCl, 10 mM imidazole, 10% (v/v) glycerol, 0.2 μ M filtered and degassed) to a volume of 100–150 mL. To lyse the cells, the cell slurry was brought to 0.1 M PMSF, 5 mM β -mercaptoethanol, 2.5 mM MgCl_2 , 0.5 mM CaCl_2 , 1 mg/mL lysozyme and 10 mg/mL DNase I and incubated on ice for 30 min. The cells were then sonicated and the lysate was centrifuged at 45,000 x g. The supernatant was loaded on 3 tandem HisTrap 5 mL Ni columns pre-equilibrated in HisBind Buffer A, and then washed extensively. When the UV signal reached baseline, the bound protein was eluted with a 505 mM imidazole bump by adding 50% HisBind Buffer B (HisBind Buffer A with 1 M imidazole). Peak fractions were evaluated by 12% SDS-PAGE and pooled. The protein was diluted 5-fold with TG0 (20 mM Tris-HCl pH 7.8, 10% (v/v) glycerol, 0.2 μ M filtered and degassed) to bring the NaCl concentration to 100 mM for ion exchange chromatography. The protein was loaded on a cation exchange column (HiTrap SP FF) pre-equilibrated with TG0 with 10% TG1000 (TG0 with 1 M NaCl). After washing, the protein

was eluted with a buffer gradient from 10% TG1000 to 50% TG1000 over 150 mL. Peak fractions were analyzed by SDS-PAGE and pooled. Protein usually eluted near 280 mM NaCl. The salt concentration was estimated from the peak and the protein was diluted to 200 mM NaCl by adding TG0. One mg of Prescission Protease was added to the protein and allowed to digest on ice at 4°C overnight. The digested protein was brought to 500 mM NaCl and 10% imidazole before loading onto a HisTrap column to remove the His tag and undigested protein. The flow through from the HisTrap column was concentrated to ~1 mL in an Amicon Ultra 15 10,000 MWCO and loaded onto a HiLoad 16/10 Superdex 200 size exclusion column pre-equilibrated in TG300D (20 mM Tris-HCl pH 7.8, 300mM NaCl, 10% (v/v) glycerol, 1 mM DTT added fresh, 0.2 μ m filtered and degassed). Fractions were analyzed by 12% SDS-PAGE, pooled and concentrated. Aliquots were flash frozen in liquid nitrogen and stored at -80°C .

SEC-SAXS (Size-Exclusion Chromatography-Small Angle X-ray Scattering)

SAXS data were collected at the Advanced Photon Source (BioCAT), beam line 18ID. The method of incorporating size-exclusion chromatography in-line with the equilibrium SAXS was carried out as described before (Mathew et al., 2004). To eliminate scattering from aggregates that could potentially make the data difficult to interpret, an in-line Superdex-200 10/300 gel-filtration column was used to purify the protein sample immediately upstream of the data collection chamber. Data acquisition was performed at a wavelength of 1.033 Å. Using a sample to detector distance of 3.5 m, we were able to access a q range of $\sim 0.006 \text{ \AA}^{-1}$ to $\sim 0.3 \text{ \AA}^{-1}$. One-second exposures were acquired through the entire duration of the SEC elution with a periodicity of 2 s. We were therefore able to use the exposures flanking the elution peak as buffer, which were averaged and subtracted from the exposures corresponding to the sample elution. Guinier approximation and pair distance distribution ($P(r)$) using PRIMUS (Konarev et al., 2003) were performed on buffer subtracted $I(q)$ versus q curves corresponding to the peak of the elution profile to obtain the radiation of gyration (R_g) and the maximum dimension (D_{max}) of the molecule. Ab initio bead models were calculated using DAMMIF, DAMAVER and DAMFILT (Franke and Svergun, 2009). Bead models from 10-20 DAMMIF processes were averaged using DAMAVER.

Single Molecule Measurements of Nucleosomes and Chd1 Proteins

Nucleosomes

Preparation of nucleosomes with octamer or hexasome histones are described in the previous sub-section. Each nucleosome consists of the 601 DNA sequence wrapped around the octamer histone, which have Cy5 labeled H2A histones. One side of the nucleosome has 80 bp of dsDNA with a biotinylated end and the other side has 3, 6, 9, or 12 bp of dsDNA and is labeled with Cy3 at the end.

Double-stranded DNA (dsDNA) Preparation

Complementary strands of oligonucleotides of random sequences were purchased from Integrated DNA Technologies (Coralville, IA). Oligos with end-labeled Cy3 dye were ordered pre-labeled. dsDNA substrates were prepared by mixing the appropriate labeled and unlabeled oligonucleotides in a 1:1 molar ratio (to avoid excess of single strands) at 10 μ M in DNA annealing buffer (10mM MgCl_2 , 10mM Tris-HCl (pH 8.0)). Double-stranded oligonucleotide mixtures were incubated at 95°C for 2 min followed by slow cooling to room temperature (at a rate of 2 degrees per minute) to complete the annealing reaction.

Nucleosome dilution buffer

50mM NaCl, 10mM Tris-HCl (pH 8.0) and 5mM MgCl_2 .

Chd1 Proteins

Preparations and bulk measurements of the full-length (Chd1-WT) and mutant Chd1 yeast proteins (Chd1-KAK, Chd1-SL) were described in the previous sub-section. 2-20nM of proteins were used in each experiments as specified.

Reaction Buffer and Condition

Buffer consisting of 20 mM HEPES (pH 7.5), 5 mM MgCl_2 , 0.1 mM EDTA, 50 mM KCl, 1 mM DTT, 5% sucrose, 0.02% Nonidet P-40 and 0.1 mg/mL BSA, was used with an oxygen scavenging system containing 1% v/v dextrose, 1 mg/ml glucose oxidase, 0.03 mg/ml catalase (Joo and Ha, 2008), and 2-mercaptoethanol (1% v/v), all items were purchased from Sigma-Aldrich (St. Louis, MO).

The measurements were performed at room temperature ($21^{\circ}\text{C} \pm 1^{\circ}\text{C}$). ATP or non-hydrolyzing ATP analogs (ATP γ S/AMP-PNP) were used in all experiments at a concentration of 1mM, unless otherwise specified.

Single-Molecule Fluorescence Assay

We used a home-built total internal reflection fluorescence microscope for single-molecule fluorescence assays. We excited the nucleosome samples containing Cy3 (donor) and Cy5 (acceptor) dyes with a solid-state 532 nm laser (75mW, Coherent CUBE) to measure the FRET signal. The emission signals were separated by using a dichroic mirror (cutoff: 630 nm) and detected by an EMCCD camera (iXon DU-897ECS0-#BV; Andor Technology). We applied FRET labeled nucleosome molecules (see above) to polyethylene glycol (PEG)-coated quartz surface via biotin-neutravidin linkage. The camera was controlled using homemade C++ program. Single-molecule traces were extracted from the recorded video file by IDL software.

Slide Surface Preparation

In all cases of single molecule experiment, passivated slides were prepared ahead of time. Briefly, both the quartz slides and coverslips were washed with methanol and acetone, etched by sonication in 1 M KOH for 30 min, flamed for 30 s, treated with aminosilane for 20 min, and coated with a mixture of 98% mPEG (m-PEG-5000, Laysan Bio, Inc.) and 2% biotin PEG (biotin-PEG-5000, Laysan Bio, Inc). The PEG-coated quartz slides are assembled into multiple-channeled imaging chamber. NeutrAvidin is added as described in (Qiu and Myong, 2016). This allows proteins or oligonucleotide to bind to the surface via the biotin-NeutrAvidin linkage.

Chd1 remodeling immobilized nucleosomes

Chd1-WT, Chd1-KAK, or Chd1-SL was mixed at 20nM with reaction buffer and added to a flow chamber that had 50-100pM nucleosomes specifically immobilized on the slide chamber surface. Excess proteins were washed away with a reaction buffer containing only ATP to observe the repositioning process in real-time. ATP concentrations ranging from 1 μ M to 1 mM were used.

Tethered Chd1 remodeling nucleosomes

Chd1 constructs containing N-terminal FLAG tags (see above) were tethered to the slide chamber surface using biotinylated anti-FLAG antibodies. Anti-FLAG tag antibody (Biotin-M2) was obtained through Sigma-Aldrich (St. Louis, MO).

For nucleosome repositioning experiments with tethered proteins, biotinylated anti-FLAG antibody (1:200 dilution) was flowed into a slide chamber with the neutravidin surface, then incubated for 5 min at room temperature. 2nM of Chd1-WT or Chd1-KAK in nucleosome dilution buffer were then added to the flow chamber and incubated for 1 min at room temperature. Then, 50-100pM of non-biotinylated nucleosomes in reaction buffer was added for the confirmation of protein-nucleosome binding (shown as corresponding Cy3 and Cy5 spots on screen), and finally, ATP in reaction buffer was added to the flow chamber to initiate the reaction.

Tethered Chd1 binding to dsDNA

For dsDNA binding experiments, slide chamber surfaces were prepared as in the case of the tethered protein, with anti-FLAG antibody and neutravidin. 10nM of Chd1-WT or Chd1-KAK were added to the slide chamber surface. Non-biotinylated dsDNA singly labeled with Cy3 ranging from 40 bp to 60 bp were added in concentrations ranging from 50pM to 2nM to observe protein-DNA binding affinity. Bound dsDNA was detected as single Cy3 spots on screen. 1mM ATP or ATP- γ S was then added (with imaging buffer) to observe any unbinding of dsDNA. (See [Table S1](#) for a complete DNA sequence information)

QUANTIFICATION AND STATISTICAL ANALYSES

Single molecule traces were analyzed with customized MATLAB functions. FRET efficiency values were calculated as a ratio between acceptor intensity and total intensity.

For dwell time analyses

Peak-to-peak dwell time (δt) for each ATP concentration was collected from multiple FRET traces (> 80) using MATLAB and fitted to exponential curves using Origin (OriginLab Corporation, Northampton, MA) to obtain the rate ($1/\delta t$) for ATP concentrations ranging from 1 μ M to 1mM. These rates can then be fitted to the Michaelis-Menten equation using the Origin software in order to find K_M , the concentration of ATP required for the reaction to reach half of the maximum rate.

For initial rate analyses

Initial FRET drop traces for nucleosome repositioning under various ATP concentrations were collected manually from individual FRET traces using MATLAB. These traces are compiled to create average FRET-time traces and fitted using Origin to obtain rate k .

For dsDNA binding analysis

Setting the maximum Cy3 spot density to 600 (> 600 = 100%), the number of Cy3 spots at various dsDNA concentration was plotted for each dsDNA-protein combination. These values were fitted into a Michaelis-Menten-like curve to obtain binding affinity of dsDNA to different Chd1 protein.

DATA AND SOFTWARE AVAILABILITY

Single Molecule FRET data acquisition and analysis package can all be obtained freely from the website (<https://cplc.illinois.edu/software/>).

IDL (<http://www.exelisvis.co.uk/ProductsServices/IDL.aspx>) and MATLAB (<https://www.mathworks.com/>) software with academic or individual licenses can be obtained from their respective software companies.

OriginLab (<http://www.originlab.com/>) software with academic or individual licenses can be obtained from the software company.